IMPRIMATUR POUR LA THÈSE

Supraconductivité en deux dimensions: propriétés spectrales du modèle de Hubbard attractif, et dynamique des vortex

de M. Massimiliano Capezzali

UNIVERSITÉ DE NEUCHÂTEL

FACULTÉ DES SCIENCES

La Faculté des sciences de l'Université de Neuchâtel sur le rapport des membres du jury,

MM. H. Beck (directeur de thèse), P. Martinoli, D. Baeriswil (Fribourg), S. Shenoy (Trieste)

autorise l'impression de la présente thèse.

Neuchâtel, le 16 décembre 1998

Le doyen:

F. Stoeckli

F. Stoeckli

DYNAMICS OF DISORDERED JOSEPHSON JUNCTION ARRAYS

M. CAPEZZALI, M. MOMBELLI, P. BERAN, H. BECK
Institut de Physique, Université de Neuchâtel, Breguet 1, CH-2000 Neuchâtel, Switzerland

ABSTRACT

We study the frequency dependence of the dielectric function $\epsilon(\omega, T)$ of a Josephson junction array in which sites or bonds are randomly removed with a given probability 1-p. The following two regimes are considered:

a) The spin wave contribution to ϵ is calculated - both for underdamped and overdamped motion - in the coherent potential approximation. The zero frequency spin wave stiffness goes to zero at a critical value of p. Depending on frequency the dynamics is governed by extended waves or by more localized fracton modes.

b) In the continuum approximation the motion of one vortex is modeled by its potential energy in a fixed distribution of circular holes. The vortex mobility is then calculated by using Mori's procedure for evaluating dynamic correlation functions.

1. Introduction

Two-dimensional Josephson junction arrays (JJA) are described theoretically by the 2-d XY model. In the presence of a magnetic field perpendicular to the plane the Hamiltonian is

$$H = \sum_{\langle ij \rangle} J_{ij} \left[1 - \cos\left(\theta_i - \theta_j - A_{ij}\right)\right], \tag{1}$$

where θ_i is the phase of the superconducting grain i, A_{ij} is proportional to the line-integral of the vector potential $\vec{A}$ over the link $< ij >$ and the sum is over the nearest-neighbor sites. The disorder in the coupling J_{ij} is given by a probability distribution φ. For bond disorder the bond probability distribution is

$$\varphi(J_{ij}) = p\,\delta\left(J_{ij} - J\right) + (1-p)\,\delta\left(J_{ij}\right), \tag{2}$$

whereas for site disorder $J_{ij} = J s_i s_j$, with the site probability distribution

$$\varphi(s_i) = p\,\delta\left(s_i - 1\right) + (1-p)\,\delta\left(s_i\right). \tag{3}$$

We use the following equation of motion for the phases θ_i including a 'local' damping term[1]

$$\alpha\ddot{\theta}_i + \eta\dot{\theta}_i = -\frac{\partial H}{\partial \theta_i}, \tag{4}$$

where α is proportional to the inverse of the capacity of the islands and η is the damping term. η is related to the normal state resistivity [2] R_0 by $\eta = R_0^{-1}(h/4\pi e)^2$. The dissipation is caused by the normal current between the superconducting grain and the (normal metal) substrate.
Various types of JJA have been studied experimentally at our institute. Disordered arrays are currently investigated. In the experiment the JJA is excited by a small ac magnetic field[3]. The conductance $G(\omega)$ is measured with the two-coil mutual-induction technique, which is related to the dielectric function $\epsilon(T, \omega)$ by

$$G(\omega) = \frac{1}{i\omega\epsilon(T,\omega)}. \tag{5}$$

We calculate the conductance in two different physical situations. We first consider the JJA at low temperature and zero magnetic field where we have a spin wave regime. Then we focus on the mobility of a vortex induced by a magnetic field.

2. Spin wave regime (low temperature and zero magnetic field)

2.1. Calculation of $G(\omega)$

Following the theory by Shenoy[4], who calculated the linear response of the thermodynamic average current I_{ij} in a link due to a small ac vector potential $\vec{A}(t)$ parallel to the x-axis, we can write the conductance as

$$G(\omega) = \frac{\Lambda}{i\omega} + \frac{\tilde{\Lambda}}{i\omega}, \tag{6}$$

where the first term is a static quantity and the second is a dynamical one. The two terms are given by

$$\begin{aligned}
\Lambda &= \frac{1}{N_l}\sum_i J_{i,i+e_x}\langle\cos(\theta_{i,i+e_x})\rangle - \frac{1}{k_B T N_l}\sum_{i,k} J_{i,i+e_x} J_{k,k+e_x}\langle\sin(\theta_{i,i+e_x})\sin(\theta_{k,k+e_x})\rangle \\
\tilde{\Lambda} &= \frac{-1}{k_B T N_l}\sum_{i,k} J_{i,i+e_x} J_{k,k+e_x} i\omega \int_0^\infty dt \langle\sin(\theta_{i,i+e_x})\sin(\theta_{k,k+e_x}(t))\rangle e^{-i\omega t},
\end{aligned} \tag{7}$$

where N_l is the total number of links and $\theta_{i,i+e_s} = \theta_i - \theta_{i+e_s}$ and θ_{i+e_s} is the phase of the nearest-neighbor in the direction $\vec{e}_s$.
To calculate $G(\omega)$ for the case of bond disorder we make the following approximations:

1. The linear dynamics of the disordered array is then approximated by the coherent potential approximation[6] (CPA). The configurational average of the spin wave propagator of the disordered array is set equal to the one of a regular array with a coupling constant $K(\omega, p)$, which depends on frequency and becomes complex. The spin -wave propagator is given by

$$\overline{G}(\vec{q}, \omega) = \frac{1}{-\alpha\omega^2 + i\eta\omega + K(\omega, p)q^2}. \tag{8}$$

2. At $T = 0$ we approximate the configurational average $\langle\Lambda\rangle_{dis}$ with the effective coupling constant $K(\omega = 0, p)$

3. In $\langle\tilde{\Lambda}\rangle_{dis}$ we approximate the term $\langle J_{i,i+e_x} J_{k,k+e_x} \sin(\theta_{i,i+e_x}) \sin(\theta_{k,k+e_x})\rangle_{dis}$ by $\langle J_{i,i+e_x} J_{k,k+e_x}\rangle_{dis} \langle \sin(\theta_{i,i+e_x}) \sin(\theta_{k,k+e_x})\rangle_{dis}$

2.2. *Results*

In CPA we have a self consistent equation[6] for the effective coupling $K(\omega, p)$

$$\frac{2}{z} K(\omega,p)(1 - u\overline{G}_{11}) - \frac{2}{z}(1 - u\overline{G}_{11}) - K(\omega,p) + p = 0, \tag{9}$$

where z is the number of nearest- neighbors, $\overline{G}_{11}$ is the on-site correlation function of the phases on the effective array and $u = -\alpha\omega^2 + i\eta\omega$. $K(\omega = 0, p)$ and u are in units of J. For u=0 the coupling K has a percolation threshold at $p_c = \frac{2}{z}$. We have a linear dependence of $K(0, p)$ on $p - p_c$ as

$$K(0,p) = \left(1 - \frac{2}{z}\right)^{-1} (p - p_c). \tag{10}$$

For $\omega \neq 0$, $K(\omega, p)$ is complex and presents three different regimes. Fig. 1 shows the results of the real part of $K(\omega, p)$ for $\alpha = 0$ (spin diffusion). At low frequency, the effective diffusion constant $\frac{1}{\eta} K(\omega, p)$ has a normal behavior. The real part of K is nearly constant and has the value of $K(0, p)$ (Eq. (10)). At a critical frequency $\omega_{c_1}(p)$, K has a crossover to a regime where its real part increases with the frequency as $\omega^{0.44}$ for p near p_c and the imaginary part becomes larger. The system presents anomalous (fractal) diffusion . The frequency $\omega_{c_1}(p)$ is proportional to $(p - p_c)^{2\nu}$ for p near p_c,where $\nu \approx 1$. The frequencies are given in units of $\frac{J}{\eta}$. The experimental values $R_0 \approx 1m\Omega$ and $J \approx 6.5K$ yield a frequency unit of 21000 Hz. For a percolation rate of p=0.55 we have $\omega_{c_1} = 160Hz$. At a higher frequencies $\omega_{c_2(p)}$ there is another crossover. The real part of K reaches the value of the average coupling ($K = Jp$). At this frequency the diffusion is over short distances (nearest-neighbors). The crossover between normal and anomalous diffusion should be seen in the inverse of the dielectric function $\epsilon(\omega, T)$. We give its behavior as function of ω and p. In Fig. 2 we plot the real part of $1/\epsilon(\omega, 0)$ as a function of the frequency ω for different probabilities p. For each value of p, we have three regimes. The critical frequencies $\omega_{c_1}(p)$ and $\omega_{c_2}(p)$ are in agreement with those found in the real part of $K(\omega, p)$. In the normal diffusion regime $Re(1/\epsilon)$ is constant. In the anomalous diffusion regime, it increases with ω and then saturates in the localized one. The CPA-approximation for site disorder is somewhat more complicated and is currently being investigated.

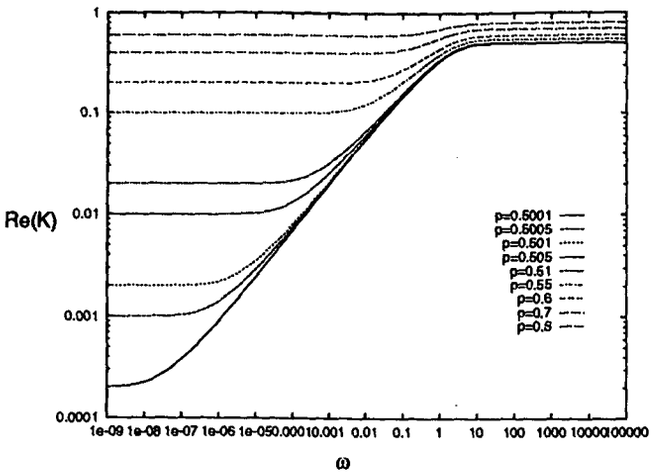

Fig. 1. Real part of the effective coupling $K(\omega, p)$ in units of J at T=0 (frequency is in units of $\frac{J}{\eta}$)

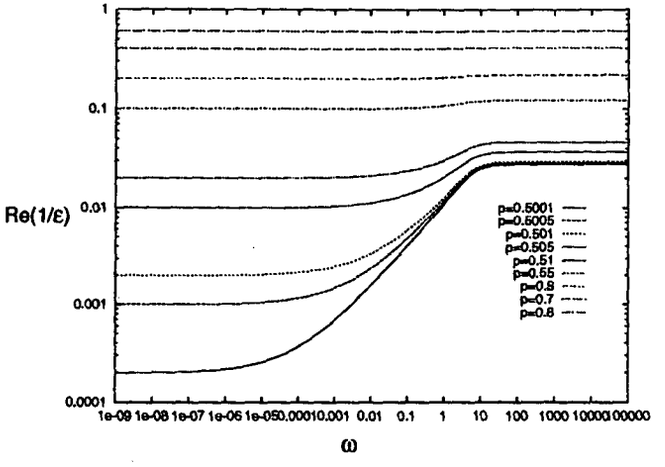

Fig. 2. Real part of $\frac{1}{\epsilon}$ at T=0 (frequency is in units of $\frac{J}{\eta}$)

3. Vortex dynamics (small magnetic field)

A single vortex in the disordered array is subject to a pinning force due to holes that have been created, by taking out sites or bonds at random. The mobility of the vortex will be calculated using an equation of motion including the pinning force and a damping term.

3.1. Holes and the related pinning energy

In the continuum approximation the regions of the planar array where bonds or sites have been taken out are represented by holes. Their statistical distribution over the sample will be modelled by considering them as impenetrable hard disks, which we assume to be circular for simplicity. No overlapping between them is admitted: when overlapping occurs, we are just in presence of a bigger hole. In the general case, holes of different radii and their partial distribution functions[7] have to be considered. Here, we present a simplified calculation based on one hole type only. Their structure factor is given by:

$$S(\vec{q}) = 1 + \frac{N}{\Omega}\int d^2 r e^{i\vec{q}\vec{r}}\left(g(\vec{r}) - 1\right), \tag{11}$$

where N is the number of holes, Ω is the surface of the entire system and $g(r)$ is the radial distribution for hard disks, the expression for which is given by Chae et al.[8]:

$$g(r) = \begin{cases} 1 + 2\left(\arccos(x) + x\sqrt{1-x^2}\,\eta_p\right) & \text{if } 1 \leq x \leq 2 \\ 0 & \text{otherwise} \end{cases} \tag{12}$$

where $x = \frac{|\vec{r}|}{2a}$, a being the radius of the hole and $\eta_p = \frac{\pi a^2}{\Omega}$ is the packing fraction. In the electrodynamic analogy, presented for example by Côté and Griffin[9], the potential energy of a vortex at rest, in the presence of holes, can be calculated by using the image-charge method and considering the holes as perfect conductors. The potential is constant when the vortex lies inside the hole and diminishes logarithmically when the latter is outside of it[10] (see Fig. 3).

3.2. Vortex equation of motion and utilization of Mori's procedure

We use the following equation of motion[1,2] for a vortex with center $\vec{R}_l$:

$$M\ddot{\vec{R}}_l + \Gamma\dot{\vec{R}}_l = -\vec{\nabla}_{\vec{R}_l}(\varphi), \tag{13}$$

where $\varphi(\vec{R}_l) = \sum_n W(\vec{r}_n - \vec{R}_l)$ is the pinning energy due to holes at positions $\vec{r}_n$, M is the vortex mass and Γ is the damping. According to Ref[1] the quantities M and Γ are proportional to the parameters α and η of Eq. (4), respectively (contrary to other techniques for deriving a vortex equation of motion[13], the "rigid trial function approach" of Ref[1] yields a finite vortex mass even in the case of a capacity to ground only) . We use Mori's procedure[11], for evaluating dynamic correlation functions. The basic variables are "vortex density" and "vortex current density" respectively defined by $\rho(\vec{r}) = \sum_l \delta(\vec{r} - \vec{R}_l)$ and $\vec{j}(\vec{r}) = \sum_l \dot{\vec{R}}_l \delta(\vec{r} - \vec{R}_l)$.

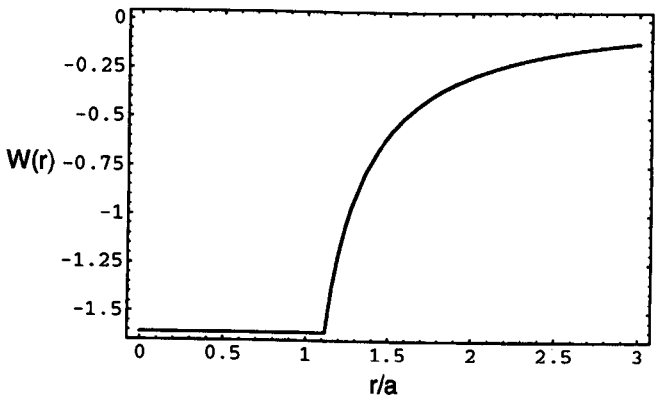

Fig. 3. Vortex pinning energy in units of J of for a hole of radius a, r being the distance separating the vortex from the center of the hole.

Since we are treating a dilute vortex system, Coulomb interaction between vortices is not considered. We then obtain the dynamic charge-charge and current-current correlation functions $\phi_{\rho\rho}$ and ϕ_{jj}:

$$\phi_{jj}(\omega) = \frac{-i\omega k_B T}{-i\omega(\Gamma + \nu(\omega)) + \vec{q}^2 k_B T}$$
$$\phi_{\rho\rho}(\omega) = \left(-i\omega + \vec{q}^2 \frac{k_B T}{\Gamma + \nu(\omega)}\right)^{-1}. \tag{14}$$

The vortex mobility is related to the zero wave-number limit of the dynamic current-current correlation[2,11] ϕ_{jj} and thus to the memory kernel $\nu(\omega)$:

$$\sigma_v(\omega) = \frac{1}{k_B T}\phi_{jj}(\vec{q} = 0, \omega) = (\Gamma + \nu(\omega))^{-1}. \tag{15}$$

In the overdamped limit (i.e. when $\alpha = 0$ and thus $m = 0$) ν obeys the self-consistent equation :

$$\nu(\omega) = (3k_B T)^{-1} \sum_{\vec{y}} \vec{y}^2 \left|\hat{\varphi}(\vec{q})\right|^2 \left(-i\omega + \vec{q}^2 \frac{k_B T}{\Gamma + \nu(\omega)}\right)^{-1}, \tag{16}$$

where $\hat{\varphi}(\vec{q})$ is the Fourier transform of the potential acting on the vortex and $\left|\hat{\varphi}(\vec{q})\right|^2 = NS(\vec{q})\left|U(\vec{q})\right|^2$ where $U(\vec{q}) = \frac{1}{\Omega}\int d^2 r e^{i\vec{q}\vec{r}} W(\vec{r})$. The zero frequency limit of ν is given by

$$\nu(0) = \frac{1}{3}\left(\Gamma + \nu(0)\right)\left(k_B T\right)^{-2} \sum_{\vec{q}} \left|\hat{\varphi}(\vec{q})\right|^2 = \left(\Gamma + \nu(0)\right) X. \tag{17}$$

3.3. *The final result: vortex mobility*

For $\omega = 0$, we obtain from Eq.'s (15) and (17):

$$\begin{aligned} \sigma_v &= \frac{1-X}{\Gamma} \\ X &= \left(\log\left(\frac{a}{a_0}\right)\frac{J}{k_BT}\right)^2 \left(\alpha\eta_p + \gamma\eta_p^3\right), \end{aligned} \tag{18}$$

where $\alpha = 3.272$, $\gamma = 4.817$ and a_0 is a cut-off , representing the vortex core, which is needed in order to avoid a diverging vortex self-energy. The packing fraction η_p is related to the probability p in Eq.'s (2) and (3) by $\eta_p = 1 - p$. The mobility of a vortex in a regular lattice ($X = 0$) is given by Γ^{-1}. The presence of defects make $X > 0$ and therefore reduces the mobility as expected. On the other hand, increasing the temperature makes X smaller and σ_v larger. The mobility goes to zero when X approaches one. This signals an effective localization of the vortex where the effect of disorder dominates over the thermal motion of the vortex. Although our calculation is too crude for quantitative predictions we can draw the following conclusions from Eq. (18):

1. We identify the hole radius a with the average radius of holes of different areas as they occur in a real sample. From a numerical simulation[12] of a disordered structure (site disorder) for various values of p, we find that $\frac{a}{a_0}$ should be around 5 when p approaches the percolation threshold p_c ($p_c = 0.593$ for a square lattice and $p_c = 0,5$ for a triangular one).

2. Taking $\frac{a}{a_0} = 5$ and $\eta_p = 0.5$ (for $p = 0.5$, i.e. near the expected percolation threshold) we find that $X < 1$ (and thus $\sigma_v > 0$) for:

$$\frac{J}{k_BT} \leq 0.601 \tag{19}$$

   For temperatures below this value, the vortex has no finite d.c. mobility anymore.

4. Summary

For low temperature and without magnetic field the effective diffusion constant $\frac{K(\omega,p)}{\eta}$, calculated by the Coherent Potential Approximation, presents a crossover between normal and anomalous (fracton) diffusion at a critical frequency $\omega_c(p)$, which is proportional to $(p-p_c)^{2\nu}$, where $\nu \approx 1$. For $\omega < \omega_c(p)$, $Re(K(\omega,p))$ is constant and its value is given by $K(\omega = 0,p)$, which presents a percolation threshold at $p_c = \frac{2}{z}$, where z is the number of nearest-neighbors. For $\omega > \omega_c(p)$, $Re(K(\omega,p))$ increases with the frequency as $\omega^{0.44}$. The real part of $\frac{1}{\epsilon(\omega,p)}$ at $T = 0$ presents a similar behavior. It is constant for $\omega < \omega_c(p)$ and increases for $\omega > \omega_c(p)$. Its imaginary part is nearly zero for $\omega < \omega_c(p)$, like in a regular array, and increases to a maximum for $\omega > \omega_c(p)$.

For a small magnetic field we calculate the mobility of a vortex in the continuum approximation, by considering the sites that have been removed, as circular holes, which act as pinning centers on the vortex. The holes are modeled as impenetrable hard disks. Using Mori's procedure to calculate dynamic correlation function, we obtain the vortex mobility, which decreases when defects are introduced; in particular a sort of localization due to the latter occurs when the disorder effect tends to dominate over the thermal motions of the vortex.

Acknowledgement

The authors thank the Swiss National Science Foundation for financial support (Proj.: 2000-040395.94/1)

References

1. H. Beck and A. Ariosa, *Sol. State Commu.* **80** (1991) 657.
2. H. Beck, *Phys. Rev. B* **49** (1994) 6153.
3. P. Martinoli, Ph. Lerch, Ch. Leemann, H. Beck, *Jpn. J. Appl. Phys.* **26** (1987) 1999.
4. S.R. Shenoy, *J. Phys. C: Solid State Phys.* **18** (1985) 5163.
5. V.L. Pokrovsky and G.V. Uimin, *Phys. Lett.* **45A** (1973) 467.
6. T. Odaki and M. Lax, *Phys. Rev. B* **24** (1981) 5284.
7. N.W. Ashcroft, in *Liquid Metals*, Inst. of Phys. Conf. Series, **30** (1972).
8. D.G. Chae, F.H. Ree ant T. Ree, *J. Chem. Phys.* **50** (1969) 1581.
9. R. Côté and A. Griffin, *Phys. Rev. B***34**(1986) 6240.
10. C.J. Lobb, D.W. Abraham, M. Tinkham, *Phys. Rev. B* **27** (1983) 150
11. J.P. Hansen and I.R. McDonald, *Theory of simple liquids* (Wiley, New York, 1976), chap 7.
12. C. Bailat, Université de Neuchâtel (Switzerland) (unpublished)
13. R. Fazio, A. Van Otterlo, G. Schön, *Europhys. Lett.* **25** (1994) 453

ELSEVIER

Physica B 222 (1996) 304–308

PHYSICA B

Dynamics of vortices in disordered Josephson junctions arrays

M. Capezzali, M. Mombelli, H. Beck*

Institut de Physique, Université de Neuchâtel, Breguet 1, 2000 Neuchâtel, Switzerland

Abstract

We have studied a two-dimensional disordered Josephson Junction Array (JJA), where sites (or bonds) have been randomly removed with a given probability $1 - p$. These defect regions of the array are modelled by a fixed distribution of holes, which are considered as being circular. We calculate the vortex mobility as a function of frequency, ω. When the holes are considered as having the same size, the former increases almost monotonically when the frequency gets higher, tending then to the value of the regular lattice as $\omega \to \infty$. For holes of different sizes, a similar behavior results from the superposition of the contribution from each family of holes.

1. Introduction

Theoretically, a two-dimensional JJA may be described by the 2-D XY model. This system undergoes the well-known Berezinskii–Kosterlitz–Thouless phase transition, which occurs at a given temperature T_{KT}, below which only bound vortex–antivortex pairs exist, whereas above this transition temperature, the pairs unbind and thus free vortices and antivortices appear. In the former temperature region, spin-wave-like excitations play a predominant role: experimental and theoretical results about this regime will be published elsewhere [1]. In this paper, we will consider the vortex mobility; our calculations can also be applied to field-induced vortices in frustrated arrays.

The paper is organized as follows: in Section 2, we introduce and explain the model we use to describe the disorder of the array and the way we find, via an electrodynamic analogy, the pinning potential, due to the holes, which is acting on the vortices. In Section 3, we present the vortex equation of motion we choose. In Section 4, we develop the Mori projector formalism used for calculating the vortex mobility, while in Section 5, we present the results we obtained and comment on different physical aspects.

2. Modelling the disorder, pinning potential

In the absence of an external magnetic field, introducing a continuous-phase field and adding an inertial term, the Hamiltonian is

$$H = \frac{J_0}{2}\int d^2r[\nabla\phi(\boldsymbol{r})]^2\Lambda(\boldsymbol{r}) + \frac{1}{2\alpha}\int d^2r[S_\phi(\boldsymbol{r})]^2\Lambda(\boldsymbol{r}). \quad (1)$$

In this expression, $S_\phi(\boldsymbol{r})$ is the momentum density associated with the phase field, α is a constant which is proportional to the site capacitance and J_0 is the coupling constant. The function $\Lambda(\boldsymbol{r})$ is introduced to take into account the disorder: it is equal to unity if the array is regular at the point $\boldsymbol{r}$, whereas it is zero if there is no site (or bond) in the array, at this point.

The regions in which $\Lambda(\boldsymbol{r})$ is equal to zero are approximated by circular "holes", which act as pinning centers for the vortices. To calculate the

*Corresponding author.

PII S0921-4526(96)00210-4

pinning potential, we use an electrodynamic analogy, as proposed, for example, by Côté and Griffin [2]: separating the phase field in a vortex (transverse) and a spin-wave component (longitudinal) and using the Hamiltonian presented above, it is possible to find four "Maxwell" equations involving a fictitious electric and magnetic field, and the charge and current density for vortices:

$$\rho(\boldsymbol{r}) = \sqrt{2\pi J_0}\sum_l \delta(\boldsymbol{r} - \boldsymbol{R}_l),\quad \boldsymbol{j}(\boldsymbol{r}) = \sqrt{2\pi J_0}\sum_l \delta(\boldsymbol{r} - \boldsymbol{R}_l)\dot{\boldsymbol{R}}_l. \tag{2}$$

$\boldsymbol{R}_l$ denotes the center of the lth vortex. The vortices can thus be described as charges of magnitude $(2\pi J_0)^{1/2}$ and the holes appear as perfect conductors (i.e. $\varepsilon_{\text{holes}} \to \infty$). Thus, we are able to calculate the pinning potential due to the holes via the image-charge method, which is particularly simple for circular holes. Defining r as the distance from the center of the hole to the vortex and taking a as the hole radius, the pinning potential due to one hole reads

$$W(r) = \pi J_0 \ln\left[\frac{r^2 - a^2}{r^2}\right] \quad (r > a),$$

$$W(r) = -\pi J_0 \ln\left[\frac{a}{a_0}\right] \quad (r < a). \tag{3}$$

Here, a_0 is the vortex core radius (which is needed to avoid a diverging vortex self-energy). The total pinning potential acting on a vortex is then (the sum runs over all holes with respective centers at $\boldsymbol{r}_n$) $\varphi(\boldsymbol{R}_l) = \sum_n W(\boldsymbol{r}_n \boldsymbol{R}_l)$.

The potential decreases as the distance from the hole to the vortex increases (for a similar result, see for example Ref. [3]), whereas inside the latter, it remains constant at its minimum value. In the electrodynamic analogy, this means that inside a perfect conductor there is a complete screening of the charge which has been inserted and thus no force is acting on it. In order to get an analytic expression for the random hole distribution, we treat the holes as impenetrable hard disks and we thus use the radial distribution function $g(r)$ for the thermodynamic equilibrium distribution of hard disks as a model. Indeed if two holes overlapped, we would replace them in our model by a larger hole of circular shape. Chae et al. [4] obtained an expression for $g(r)$, which reads

$$g(r) = \begin{cases} 1 + 2(\arccos(x) + x\sqrt{1 - x^2})\eta_p & \text{if } 0.5 \leqslant x \leqslant 1, \\ 0 & \text{otherwise.} \end{cases} \tag{4}$$

Here, $x = r/4a$ and η_p is the packing fraction (i.e. the ratio of the surface of the holes to the total area of the system). The corresponding structure factor $S(\boldsymbol{q})$ is shown in Fig. 1. The Fourier transform of the pinning potential may be written as $\varphi(\boldsymbol{q}) = NS(\boldsymbol{q})W(\boldsymbol{q})$, where $W(\boldsymbol{q})$ is proportional to a modified Bessel function of order zero (i.e. to $K_0(qa)$); the latter is thus already negligible for values of qa larger than two. This permits us to apply a cut-off on the partial structure factor, i.e. we consider only the part of it which lies before this function reaches its first local maximum (occurring at $qa \cong 2.8$) and assume a quadratic form for it, while the remaining part (i.e. for $qa > 2.8$) is put to zero. The structure factor which will be used later is found by performing a quadratic numerical fit:

$$S(q) = \begin{cases} (1 - 1.64\eta_p^2) + 0.275(qa\eta_p)^2 & \text{if } qa < 2.8, \\ 0 & \text{otherwise.} \end{cases}$$

In the general case, i.e. when holes of different sizes represent in the JJA, we must introduce partial structure factors, called $S_{ss'}(\boldsymbol{q})$, the index s being related to the sth hole family ($s = 1$ for the holes

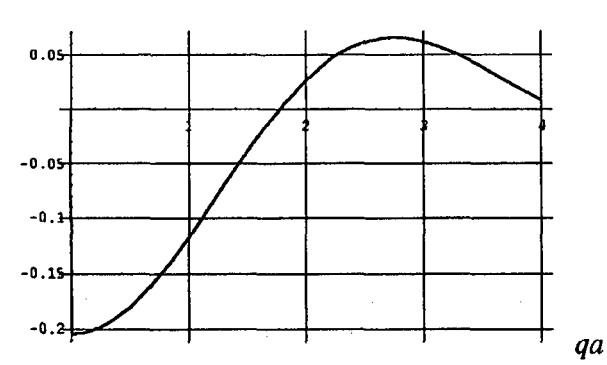

Fig. 1. Structure factor versus wave number q, resulting from $g(r)$, Eq. (4).

created by the removal of only one site, and so on). The diagonal partial structure factors ($s = s'$) have the same form as above, but with a replaced by a_s (i.e. the radius which characterises the holes belonging to the sth family) and η_p by the partial packing fraction of the sth family, η_s.

Considering circular holes is probably a good approximation for the small holes (only a few sites removed), while for bigger ones, which are mostly of ramified structure [5], we are obliged to define an averaged area and transform it in a corresponding disk area (i.e. thus defining a_s as an average radius for the sth family). This implies that our model should be applicable if the JJA is not too close to the percolation threshold (where a non-negligible number of very big holes could appear).

3. Vortex dynamics

We now introduce an equation of motion for the vortex. Using a rigid trial function approach and starting from a discrete Hamiltonian equivalent to Eq. (1), Beck and Ariosa [6] found a vortex equation of motion, which reads

$$M_v\ddot{\boldsymbol{R}}_l + \Gamma\dot{\boldsymbol{R}}_l = -\nabla_{R_l}(\varphi). \tag{5}$$

M_V is the vortex mass, which is proportional to the constant α, and Γ is the damping constant. The right-hand side of Eq. (5) is the gradient of the potential to which the vortex is subjected; since we are considering only one vortex (i.e. there is no Coulomb interaction with other vortices) φ is the pinning potential we found in Section 2. For the type of JJAs which have been studied in Refs. [7, 8], M_V can be neglected, because the arrays behave as overdamped systems. We will adopt this limit here too.

4. Mori's formalism, correlation functions and mobility

We adopt Mori's formalism [9] to find the dynamic "charge density–charge density" and "current density–current density" autocorrelation functions, respectively, named $\phi_{\rho\rho}(\boldsymbol{q}, \omega)$ and $\phi_{jj}(\boldsymbol{q}, \omega)$. Here, ω is the driving frequency which is applied to the JJA [8, 10]. We start defining two dynamical variables, $A_1(\boldsymbol{q}) = \rho(\boldsymbol{q})$ and $A_2(\boldsymbol{q}) = \hat{q}\cdot\boldsymbol{j}(\boldsymbol{q})$, which are obtained from the expressions (2) by Fourier transforming. Replacing, as usual, the projectors showing up in the time evolution of the relaxation kernels [9] by unity and using Eq. (5) we finally find

$$\phi_{\rho\rho}(\omega) = \left[-\mathrm{i}\omega + q^2\frac{k_BT}{\Gamma + \nu(\omega)}\right]^{-1},$$

$$\phi_{jj}(\omega) = \frac{-\mathrm{i}\omega k_BT}{-\mathrm{i}\omega(\Gamma + \nu(\omega)) + q^2k_BT}. \tag{6}$$

In this expression, $\nu(\omega)$ is the memory (relaxation) kernel, which contains the interaction of the vortex with the holes, via the Fourier transform of the pinning potential found above:

$$\nu(\omega) = (3k_BT)^{-1}\sum_q q^2|\varphi(\boldsymbol{q})|^2\left[-\mathrm{i}\omega + q^2\frac{k_BT}{\Gamma + \nu(\boldsymbol{q},\omega)}\right]^{-1}. \tag{7}$$

We then use the Kubo relation to express the link between the vortex mobility to the charge density–charge density correlation function [7], i.e.

$$\sigma_v(\omega) = \lim_{q\to 0}(k_BT)^{-1}\phi_{jj}(\boldsymbol{q},\omega) = [\Gamma + \nu(\omega)]^{-1}$$

$$\equiv [\gamma(\omega)]^{-1}. \tag{8}$$

5. Results and comments

In a previous paper [11], we obtained the vortex mobility in the static limit ($\omega \to 0$) and assuming all the holes had the same size. We concluded that the presence of holes lowers the vortex mobility and showed that an effective "locking" of the vortex appears when the effect of disorder dominates over the thermal motion of the vortex. In particular, using the hole distribution obtained in a numerical simulation of a site-disordered structure near the percolation threshold [5], we found that for temperatures below the limit $J_0(k_BT)^{-1} \leqslant 0.601$, the vortex has no finite DC mobility anymore. We perform here the generalizations to the frequency-dependent vortex mobility in a disordered JJA,

where holes of different sizes are present. Using expressions (6), (7) and (8) and calculating explicitly the Fourier transform of the potential, we find the general expression for the inverse of the vortex mobility, $\gamma(\omega)$,

$$\gamma(\omega) = \Gamma + \gamma(\omega)\left[\frac{2\pi^2 J_0^2}{3(k_B T)^2}\sum_{s,s'}\int dq \frac{\sqrt{\eta_s \eta_{s'}} q^3 a_s a_{s'} S_{ss'}(q)}{q^2 + \dfrac{-i\omega\gamma(\omega)}{k_B T}}\right.$$

$$\left.\times \ln\left[\frac{a_s}{a_0}\right]\ln\left[\frac{a_{s'}}{a_0}\right]K_0(qa_s)K_0(qa_{s'})\right], \qquad (9)$$

where we recognize $S_{ss'}(q)$, i.e. the hole partial structure factors and the double sum which runs over all hole families. At this point, we apply an approximation, assuming that the contribution of the off-diagonal partial structure factors is zero; Rosenfeld [12] calculated the latter for a system containing two families of holes and his results show that the off-diagonal partial structure factor behaves differently from the diagonal ones: the former weakly oscillate around zero and their magnitude is much smaller than the one of the latter.

We now use a perturbative approach to find an expression for the vortex mobility: the correlators showing up in the memory kernel are approximated by their lowest order form, i.e. $\gamma(\omega) = \Gamma$ on the right-handside of Eq. (9). Posing

$$X(0) = \left(\frac{J_0}{k_B T}\right)^2 \sum_s \left(\ln\left(\frac{a_s}{a_0}\right)\right)^2 \eta_s (3.272 - 4.817\eta_s^2),$$

we finally find the general expression for the frequency-dependent vortex mobility:

$$\sigma_v(w) = \Gamma^{-1}[(1 - X(0) + A(\omega)) + iB(\omega)],$$

where

$$A(\omega) = \sum_s \left(\ln\left(\frac{a_s}{a_0}\right)\frac{J_0}{k_B T}\right)^2$$

$$\times\left[3.272\eta_s\left[\frac{\omega^2 a_s^4 \Gamma^2/(k_B T)^2}{\omega^2 a_s^4 \Gamma^2/(k_B T)^2 + 1.5}\right]^{1/4}\right.$$

$$+ \eta_s^3\left(0.549\left[\frac{\omega^2 a_s^4 \Gamma^2/(k_B T)^2}{\omega^2 a_s^4 \Gamma^2/(k_B T)^2 + 15}\right]^{1/2}\right.$$

$$\left.\left. - 5.366\left[\frac{\omega^2 a_s^4 \Gamma^2/(k_B T)^2}{\omega^2 a_s^4 \Gamma^2/(k_B T)^2 + 1.5}\right]^{1/4}\right)\right],$$

$$B(\omega) = \sum_s \left(\ln\left(\frac{a_s}{a_0}\right)\frac{J_0}{k_B T}\right)^2$$

$$\times\left[-3.619\eta_s\sqrt{\frac{\omega a_s^2 \Gamma}{k_B T}}e^{-1.5\sqrt{\omega a_s^2 \Gamma/k_B T}}\right.$$

$$+ \eta_s^3\left(5.935\sqrt{\frac{\omega a_s^2 \Gamma}{k_B T}}e^{-1.5\sqrt{\omega a_s^2 \Gamma/k_s T}}\right.$$

$$\left.\left. - 0.507\frac{\omega a_s^2 \Gamma}{k_B T}e^{-1.21\sqrt{\omega a_s^2 \Gamma/k_s T}}\right)\right].$$

If there were only one hole family, then the sum over s would disappear and the packing fraction would just be η_p.

In Fig. 2, we compare the real part of the vortex mobility for two different percolation rates (corresponding respectively to $p = 0.9$ and $p = 0.8$) versus the driving frequency. These results are obtained using the hole distribution of Ref. [5] and defining an average radius, a_s, for all respective holes families; they give rise to the following physical comments.

(a) When just one family of holes is considered, a crossover appears between two different frequency regimes. In the low-frequency region, the real part of the vortex mobility is reduced by the presence of defects; the smaller the driving frequency is, the smaller the mobility. After the crossover, we penetrate in the high-frequency region, where the vortex mobility gradually tends to the value of the regular lattice, i.e. Γ^{-1}, as ω becomes large. We can understand this result in the following way: at very small driving frequencies, the timescale which is imposed by the external excitation is rather large; this means that the vortex has much time to "travel" across the array and the probability to be trapped by a hole (or by many holes succesively) is thus large. At high driving frequencies, in contrary, the oscillation time is rather small and this implies that the vortex will typically

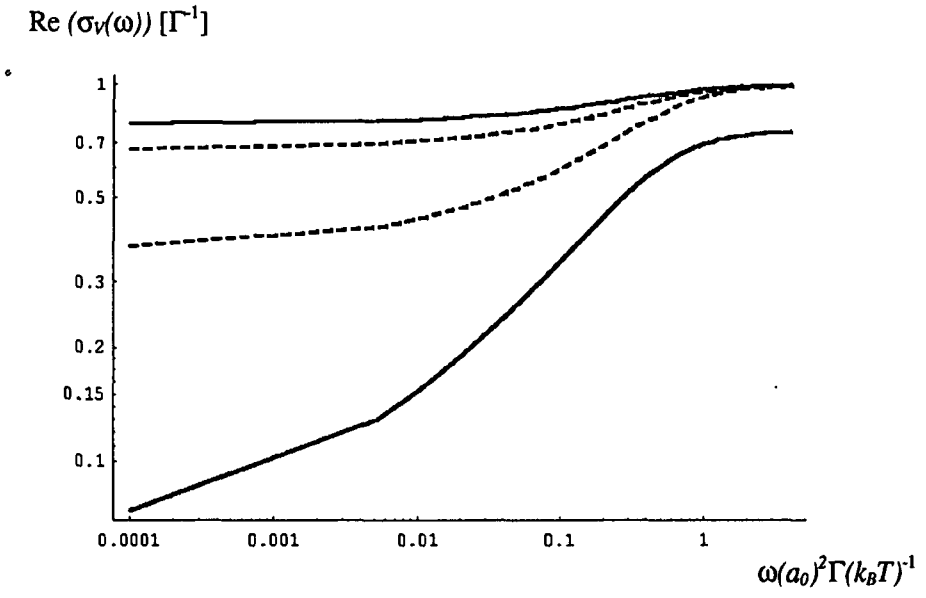

Fig. 2. Real part of the vortex mobility for two different percolation rates versus driving frequency. Starting from below, we present the two curves obtained $p = 0.8$, while the two curves above have been calculated by taking $p = 0.9$. The dashed lines are related to the calculations for just one hole family (2 sites removed), while the continuous ones are the graphic result when we consider many families of holes.

oscillate in a very small region, without being trapped by a hole.

(b) The imaginary part of the mobility, which is linked to the dispersion that the vortex experiences, is not shown on Fig. 2. It is zero in the static limit, grows monotonically until it reaches a maximum (which occurs in the middle of the transition of the real part). Thereafter, the imaginary part falls down to zero again.

(c) When we consider many families of holes, a crossover regime appears also between the two frequency limits in the real part of the vortex mobility. The latter shows to be the sum of the contributions of the different families; we find that each one presents a specific crossover frequency, which varies as the inverse square of the average radius a_s.

(d) According to the numerical simulations of Ref. [5], we only had to consider three hole families for $p = 0.9$, while for $p = 0.8$ we had to take account of eight families. This means that, for these percolation rates only very few big holes exist and that we can neglect them. Analyzing the contribution of the different families for $p = 0.8$, we find that although there are many more very small holes (1 or 2 sites removed) than bigger ones, the largest contributions to $\gamma(\omega)$ come from the holes created by removing 4 and 5 sites: the number of the latter is small but their pinning potential is stronger than the one of the small holes.

Acknowledgements

The authors would like to thank the Swiss National Science Foundation for supporting this work, under project 2000-040395.94/1.

References

[1] P. Martinoli et al., to be published.
[2] R. Côté and A. Griffin, Phys. Rev. B 34 (1986) 6240.
[3] C.J. Lobb, D.W. Abraham and M. Tinkham, Phys. Rev. B 34 (1986) 6240.
[4] D.G. Chae, F.H. Ree and T. Ree, J. Chem. Phys. 50 (1969) 1581.
[5] C. Bailat, Diploma Thesis, University of Neuchâtel, Switzerland.
[6] H. Beck and D. Ariosa, Solid State Commun. 80 (1991) 657.
[7] H. Beck, Phys. Rev. B 49 (1994) 6153.
[8] R. Théron et al., Phys. Rev. Lett. 71 (1993) 1246.
[9] H. Mori, Prog. Theor. Phys. 34 (1965) 399.
[10] P. Martinoli et al., Japanese J. Appl. Phys. 26 (1987) 1999.
[11] M. Capezzali et al., in: Macroscopic Quantum Phenomena and Coherence in superconducting Networks, eds. C. Giovanelli and M. Tinkham (World Scientific, Singapore, 1995) p. 270.
[12] Y. Rosenfeld, Phys. Rev. B 42 (1992) 5978.

Regime Interpretation of Anomalous Vortex Dynamics in 2D Superconductors

Massimiliano Capezzali,[1] Hans Beck,[1] and Subodh R. Shenoy[2]
[1]*Institut de Physique, Université de Neuchâtel, Rue A.L. Breguet 1, 2000 Neuchâtel, Switzerland*
[2]*Condensed Matter Physics Group, International Centre for Theoretical Physics, 34100 Trieste, Italy*
(Received 15 March 1996)

Low-frequency dynamic impedance $[\sigma^{-1}(\omega,T) \equiv (\sigma_1 + i\sigma_2)^{-1}]$ measurements on Josephson junction arrays found that $\sigma_1 \sim |\ln\omega|$, $\sigma_2 \sim$ const. This implies anomalously sluggish vortex mobilities $\mu_V(\omega) \sim \sigma_1^{-1}$, and is in conflict with general dynamical scaling expressions. We calculate (a) $\sigma(\omega,T)$ by real-space vortex scaling and (b) $\mu_V(\omega)$ using Mori's formalism for a screened Coulomb gas. We find, in addition to the usual critical (large-ω) and hydrodynamic (low-ω) regimes, a new intermediate-frequency scaling regime into which the experimental data fall. This resolves the above mentioned conflict and makes explicit predictions for the scaling form of $\sigma(\omega,T)$. [S0031-9007(96)02147-3]

PACS numbers: 74.50.+r, 05.90.+m, 74.60.Ge

The dynamic conductivity of superconductors $\sigma(\omega,T) \equiv \sigma_1 + i\sigma_2 \equiv |\sigma|e^{i\phi_\sigma}$, including high-$T_C$ materials and Josephson junction arrays (JJA), has been the focus of much recent interest [1–4]. Dynamical scaling forms, $\sigma = \xi^{2+z-d}S_\pm(Y^{-1})$, $\phi_\sigma = \Phi(Y^{-1})$ were proposed by Fisher *et al.* [1] and Dorsey [2], where z is the dynamic exponent, and $Y \sim 1/\omega\xi^z$. The results apply [1,2] also for the vortex-unbinding Kosterlitz-Thouless (KT) transition in $d = 2$ [5], ξ being the vortex screening length. The scaling functions Φ_σ and S_+ (S_-) have well-defined limits in the hydrodynamic ($Y \gg 1$) and critical ($Y \ll 1$) regimes, e.g., $\sigma_1 \to \xi^2$, $\sigma_2 \to 0$ in the $Y \to \infty$, dc limit. 2D JJA's [6] are clean, controllable 2D superconductors, and should be ideal systems to display the universal dynamic scaling behavior and limits.

Remarkably, however, low-frequency dynamic impedance (σ^{-1}) measurements [4] on 2D SNS triangular-lattice JJA's with a (field-induced) vortex screening length ξ, find $\sigma_1 \sim |\ln\omega|$, $\sigma_2 \sim$ const, in conflict with dynamic scaling limits. This also implies anomalously sluggish low-frequency vortex mobilities, $\mu_V(\omega) \sim \sigma_1^{-1} \sim 1/|\ln\omega|$ going to zero for $\omega \to 0$. σ is related to the dynamic dielectric function $\epsilon(\omega)$: $\sigma \sim iY/\epsilon(\omega)$. Surprisingly, Minnhagen's phenomenology (MP) for $\epsilon(\omega)$, described below, and related simulations support this anomalous behavior, but understanding the apparent breakdown of dynamical scaling, in the very arena where one might expect its clear verification, is of central importance.

In this Letter, we reconcile these results, by a "regime interpretation" [7] defined by the ratio $Y = (r_\omega/\xi)^2$ of the (squares of the) frequency-dependent diffusive probe length [8] $r_\omega = \sqrt{\Gamma_0/\omega}$ and the screening length ξ. Here, Γ_0 is a junction-determined phase diffusion rate, the lattice constant is unity, and we consider weak screening and probes over several lattice constants: $\xi \gg 1$, $r_\omega \gg 1$. We (a) recalculate $\sigma(\omega,T)$ by a real-space scaling [9], with an improved treatment of intermediate-scale screening and (b) evaluate the vortex mobility μ_V using Mori's formalism for a screened Coulomb gas [10]. Three probe-scale regimes emerge. (I) Probing free-vortex scales ("low" frequencies) $r_\omega \gg \xi$, in a "hydrodynamic" region, Drude behavior with the correct [1,2] dc conductivity, $\sigma_1(\omega \to 0,T) \sim \xi^2$, is recovered. (II) At intermediate scales/frequencies, $r_\omega \lesssim \xi$, in a new "precritical" region, MP-like behavior, $\sigma_1 \sim |\ln\omega|$ is found. (III) Probing bound pair scales ("high" frequencies) $r_\omega \ll \xi$ in a "critical" region extending from just above T_{KT} to $T = 0$, a scale-dependent vortex damping $\sim\sigma_1 \sim (r_\omega/\ln\omega)^2 \sim [\omega(\ln\omega)^2]^{-1}$ is found, corresponding to large pairs moving in a logarithmically interacting viscous medium of smaller pairs. The results of $\omega \to 0$, $T \to T_{KT}^+$ thus depend on the order of the limits. The ratio $R_\sigma = \sigma_1(\omega,T)/\sigma_2(\omega,T) \equiv \cot\phi_\sigma$ at $Y = 1$ interpolates between Drude ($R_\sigma = 1$) and MP ($R_\sigma = 2/\pi$) signatures [11], as ω increases from zero, or T increases from T_{KT}^+. As a satisfying byproduct of calculation (a), the MP-like expressions emerge as approximations to the σ/ξ^2 scaling function, valid in regime II. Calculation (b) demonstrates that the general results are independent of the details of JJA dynamics, and depend only on Coulomb gas screening properties. Local spin-wave damping mechanism specific to SNS arrays [10,12] could play an additional role in producing anomalous behavior, widening regime II. But both SNS and SIS arrays should show all three regimes in principle, with different relative sizes of regimes I and II, coming from very general considerations.

Two different physical circumstances yield a nonzero free vortex density, and thus finite ξ: (i) For zero external flux, and $T > T_{KT}$, $\xi^{-1} = \xi_+^{-1}(T) \sim e^{-(T-T_{KT})^{-1/2}} \neq 0$ above transition, $T > T_{KT}$; while $\xi^{-1} = 0$ for $T < T_{KT}$. (ii) Flux-induced vortices of concentration $f \ll 1$ [4] (too dilute to form a stable lattice) can form a one-component plasma with a screening length ξ, given by the Debye expression $\xi^{-1} = \xi_D^{-1}(f) = (4\pi^2 f/\overline{T})^{1/2} \neq 0$, corresponding to "above transition" for any T.

We now sketch the MP ideas [11], originally developed to describe $\sigma(\omega,T)$ structures at $T=T_\omega>T_{\rm KT}$, where $\xi_+(T_\omega)=r_\omega$. The zero-wave-vector conductivity $\sigma(\omega,T)$ is proportional to the corresponding (inverse) dielectric constant: $\sigma(\omega,T)/\sigma_0K_0\xi^2=iY[\varepsilon_V(k=0,\omega,T)]^{-1}$, where σ_0 is a conductivity scale and K_0 the bare vortex coupling. In MP, the real part $\Re[\varepsilon_V(k=0,\omega,T)^{-1}]$ of this zero-wave-vector dynamic function is approximated by the zero-frequency static function, $\Re[\varepsilon_V(k,\omega=0,T)^{-1}]$, evaluated at the probe scale, $k=r_\omega^{-1}$. The imaginary part, $\Im[\varepsilon_V(k=0,\omega,T)^{-1}]$ is found from the Kramers-Kronig (KK) relations, that produce a $\ln Y$ dependence. Thus [11], with $\varepsilon_V(k=0,\omega,T)^{-1}=\vec{k}^2/(\vec{k}^2+\xi^{-2})$,

$$\frac{\sigma_2}{\sigma_0K_0\xi^2}=\frac{Y}{Y+1},\qquad \frac{\sigma_1}{\sigma_0K_0\xi^2}=\frac{2}{\pi}\frac{Y^2\ln Y}{Y^2-1}. \quad (1)$$

At $Y=1$, $R_\sigma=2/\pi$ [i.e., $\phi_\sigma=\arctan(\pi/2)$], an MP signature. The dynamical scaling limits [1,2] in the $Y\ll 1$ critical regime, both above and below $T_{\rm KT}$, are $\sigma_1\sim\sigma_2\sim 1/\omega$ (independent of ξ), $\Phi_\sigma=\pi/2$. In the $Y\gg 1$ hydrodynamic regime, for $T>T_{\rm KT}$ ($T<T_{\rm KT}$), one finds $\sigma_1\sim\xi^2$, $\sigma_2\sim 0$, $\Phi_\sigma\sim 0$ [$\sigma_1\sim\delta(\omega)$, $\sigma_2\sim 1/\omega$]. Equation (1) for MP has very different limits; however, $\sigma_1\sim\xi^2Y^2|\ln Y|$, $\sigma_2\sim 1/\omega$ for $Y\ll 1$; and $\sigma_1\sim\xi^2|\ln Y|$, $\sigma_2\sim\xi^2$ for $Y\gg 1$. (Note that the $Y\gg 1$ limit, for $\xi=\xi_+(T)$ fixed, $\omega\to 0$, implies infinite dc conductivity, *above* $T_{\rm KT}$.) We now outline our two complementary calculations, with details elsewhere [7], showing that MP-like behavior emerges in an intermediate regime II, rather than in the scaling form regimes I, III.

(A) Real-space vortex scaling and $\sigma(\omega,T)$.—The total (dimensionless) JJA bond current $I^{\rm tot}_{\mu i}$ ($\mu=x$, y directions) is a sum of Josephson or super- ($\sim\sin\Delta_{\mu\theta_i}$), phase-slip or normal- ($\sim\Delta_\mu\dot\theta_i$), and noise currents, and is conserved at every 2D lattice site i. If we ignore capacitive charge buildup on grains,

$$\sum_\mu\Delta_\mu I^{\rm tot}_{\mu i}=\sum_\mu\Delta_\mu\{\overline{T}^{-1}\sin[\Delta_\mu\theta_i-\dot A_{\mu i}(t)] + \nu_0^{-1}[\Delta_\mu\dot\theta_i-\dot A_{\mu i}(t)]+f_{\mu i}(t)\}=0. \quad (2)$$

Here, $\nu_0\equiv(2eR_JI_J/\hbar)\overline{T}\equiv\Gamma_0\overline{T}$, $\overline{T}^{-1}\equiv(\hbar I_J/2ek_BT)$, and I_J, R_J are the junction critical current and the effective shunt resistance [9,13], for the SNS/SIS array. The random noise current obeys $\langle f_{\mu r}(t)f_{\mu' r'}(t')\rangle=(2/\nu_0)\delta_{\mu\mu'}\delta_{rr'}\delta(t-t')$. The JJA grain phases are $-\pi<\theta_i\le\pi$, and the external transverse vector potential $A_{\mu i}(t)=A_{\mu i}(\omega)e^{-i\omega t}$ is weak. Inverting the Laplacian $\vec{\Delta}^2$ on $\dot\theta_i$, the Langevin dynamics equation for the phase is [9,14]

$$\dot\theta_r=-\sum_{r'}\tilde G_{rr'}\left[\nu_0\frac{\partial\beta H}{\partial\theta_r}+\hat F_{r'}(t)\right], \quad (3)$$

where $\beta H=-\frac{1}{T}\sum_{\mu,r}\cos[\Delta_\mu\theta_r-A_\mu(t)]$, $\tilde G_{rr'}=G_{rr'}-G_{rr}$ is the 2D lattice Green's function (with singular part subtracted), and $\langle\hat F_r(t)\hat F_{r'}(t')\rangle=2\nu_0\tilde G_{rr'}\delta(t-t')$.

The dynamic conductivity calculation [9] yields $\sigma_{\mu r,\mu' r'}\equiv\overline{\sigma}_{\mu r,\mu' r'}+\tilde\sigma_{\mu r,\mu' r'}$. Here, $\overline{\sigma}$ is the usual superfluid response, which at long wavelengths is $(\overline{\sigma}/\sigma_0)=\pi K_\infty\Gamma_0\delta(\omega)+iK_\infty(\Gamma_0/\omega)$. With $\langle\rangle_0$ denoting an average with weight $P_0=e^{-\beta H[\Delta\theta-A(t)]}$, $\tilde\sigma$ can be written as

$$\frac{\tilde\sigma_{\mu r,\mu' r'}}{\sigma_0}\sim\overline{T}^{-2}\int_0^\infty e^{i\omega t}\langle\sin\Delta_\mu\theta_r e^{-\hat L_0t}\sin\Delta_{\mu'}\theta_{r'}\rangle_0\,dt. \quad (4)$$

As before [9], we extract vortices by a dual transform, do a Gaussian truncation on spin waves, and find that the effect of the Fokker-Planck "propagator" $e^{-\hat L_0t}$ is to produce a correlation angle decay as $e^{-\Gamma_0t}$. The correlation $\tilde\sigma_{\mu r,\mu' r'}$ can be expressed as the projection (through derivatives) of the vortex partition "generating function," with separated "test charges" at μr and $\mu' r'$. Doing the time integral in Eq. (4), the $e^{-\Gamma_0t}$ factors lead to a test charge $(i\omega/\Gamma_0)/(1-i\omega/\Gamma_0)$ at $\mu' r'$ in the partition function. The logarithmic potential, $\vec{\Delta}^2U_0(R/a)=+2\pi\delta_{\vec R,\vec 0}$ and dipolar ($\xi^{-1}=0$) scaling equations [5] can be generalized [7] to include weak ($\xi^{-1}\ll 1$) monopolar screening of a, $a+da$ dipole binding, approximated by a potential $\vec{\Delta}^2U(R/a)=+2\pi g_l\delta_{\vec R,\vec 0}$. Real-space integration of pairs of separation a, $a+da$ can then be done, as usual [5], producing the renormalized coupling K_l that obeys KT scaling equations. Since vortex damping is across the junctions in the array, it is scale dependent, $\Gamma_0\to\Gamma_l\equiv\Gamma_0/a^2$ ($z=2$), where $a\equiv e^l$, so the frequency-dependent test charge is $(i\omega a^2/\Gamma_0)/(1-i\omega a^2/\Gamma_0)$ [13]. After projection, this provides a dynamic Drude factor, at scale $a\equiv e^l$, that weights the incremental, (static) scaling contributions, $d(K_lg_l)$. The KK relations are thus automatically satisfied.

With a partial integration, the long-wavelength conductivity $\tilde\sigma(\omega)$ is then, finally, an integral over all pair contributions, with a range of length (and time) scales

$$\frac{\tilde\sigma(\omega)}{\sigma_0\xi^2}=Y\int_0^\infty dl\,K_lg_l\left[\frac{d}{dl}\frac{(a/r_\omega)^2}{1-i(a/r_\omega)^2}\right]. \quad (5)$$

For $a\ll 1$, $g_l\simeq 1$, and for $a\gg 1$, g_l is the Debye dielectric constant $q^2/(q^2+\xi^2)$ at a scale $q\sim a^{-1}$: $g_l\simeq[1+(a/\xi)^2]^{-1}$. The dominant monopole effect on $\sigma(\omega)$ is the explicit g_l factor, representing a scale-dependent reduction of far-off fields, as seen by a, $a+da$ dipoles. There is a smooth crossover from dipolar ($a\ll\xi$, regime III) to monopolar ($a\gg\xi$, regime I) screening with probes $r_\omega\sim a$, and with mutual ($a\sim\xi$, regime II) screening in between. Previously, we had matched regime I/III behavior directly [9] effectively taking g_l to be a step function, and suppressing the intermediate regime. For external free-vortex screening [$\xi=\xi_D(f)$], $g_l=1/[1+(a/\xi)^2]$ throughout.

Changing variables in Eq. (5), $a/\xi\to a$ we see $\tilde\sigma(\omega,T)$ is a function of Y, with only logarithmic deviations $\sim l_\xi\equiv\ln\xi$, from the limits of the integral and in $K_l\to K_{l+l_\xi}$.

For $\xi \propto \xi_D(f) \sim \sqrt{f}$, this implies a quasiuniversality [1] in $Y \sim f/\omega$, as found [4]. The imaginary part $\tilde{\sigma}_2$ of Eq. (5) has a function peaked at $a^2/\xi^2 = Y$ in square brackets, multiplying a roll-off function. By rapid roll-off and sharp-peaking estimates, the *total* σ_2 is estimated as ($l_\omega \equiv \ln r_\omega$)

$$\frac{\sigma_2}{\sigma_0 \xi^2} \approx Y\left[K_{l\xi}\frac{Y^{-2}}{1+Y^{-2}}, K_{l\omega}\frac{Y^{-1}}{1+Y^{-1}}, K_{l\omega}\right], \quad (6)$$

in the regimes I, II, and III, respectively, or $Y \gg 1$, $Y \leq 1$, $Y \ll 1$. Note in regime III, the ξ^2 factor cancels, and [9] $\sigma_2/\sigma_0 \approx K_{l\omega}/\omega$ with the correct superfluid kinetic inductance limit K_∞/ω, for $T < T_{KT}$, $\omega \to 0$. The real part of the total conductivity, apart from the $\delta(\omega)$ term, (using KK relations in regime II, where the integral is harder to estimate) is

$$\frac{\sigma_1}{\sigma_0 \xi^2} \approx \left[\frac{K_{l\xi}}{1+Y^{-2}}, \frac{2}{\pi}\frac{K_{l\omega}\ln Y}{1-Y^{-2}}, -\frac{1}{2}\frac{dK_{l\omega}}{dl_\omega}\frac{\arctan Y^{-1}}{Y^{-1}}\right] \quad (7)$$

in regimes I, II, and III, respectively. The σ/ξ^2 results of Eqs. (6) and (7) agree with the scaling limits [1,2] of $S_\pm(Y^{-1})$ and $\phi_\sigma(Y)$ in regimes I and III. In regime II, with dipolar screening neglected ($K_{l\omega} \to K_0$), σ/ξ^2 is of the MP form, Eq. (1). With [5] $K_l \sim K_\infty + l^{-1}$ in regime III, $\sigma_1/\sigma_0 \sim (\Gamma_0/\omega)/l_\omega^2$ for all $T < T_{KT}$ reflecting the KT "critical line," in the dynamics; the phase angle [1,2] $\phi_\sigma = \arctan(\sigma_2/\sigma_1) \to \pi/2$, as $\omega \to 0$.

(B) *Coulomb gas vortex dynamics.*—It is important to directly calculate the Coulomb gas vortex "charge" mobility [10] (for $\xi^{-1} \neq 0$) in a way that is manifestly independent of the details [13] of JJA dynamics, but shows the two frequency regimes I and II (since dipolar screening is not included, regime III will not appear). The overdamped equation of motion for a charge $+1$ is $\Gamma_V \dot{\vec{R}}_l = -\sum_{j\neq i} e_j \vec{\nabla} V(\vec{R}_i - \vec{R}_j)$, where the potential between charges ($e_j = \pm 1$) in Fourier space is $V(\vec{q}) = (\vec{q}^2)^{-1}$ and Γ_V is a friction coefficient. We use Mori's formalism [10,15] to relate $\mu_V(\omega)$ to the correlation function $\Phi_{\rho\rho}(\vec{q},\omega)$ for the vortex charge density $\rho(\vec{R}) = \sum_i e_i \delta(\vec{R} - \vec{r}_i)$. The inverse mobility of a given particle or effective viscosity function is the sum of the bare friction coefficient and a contribution that is related to the forces from all other particles:

$$\mu_V^{-1}(\omega) = \Gamma_V\left[1 + (k_BT)^{-1}\sum_{\vec{q}} |\vec{q}V(\vec{q})|^2 \Phi_{\rho\rho}(\vec{q},\omega)\right]. \quad (8)$$

In order to evaluate $\Phi_{\rho\rho}(\vec{q},\omega)$ we make the usual approximations [10] (neglect of the "Mori projector" and decoupling higher correlations in terms of $\rho(\vec{q})$ and $n(\vec{q})$, the number density Fourier component). One obtains

$$\Phi_{\rho\rho}(\vec{q},\omega) = \frac{S_\rho(\vec{q})}{i\omega + \frac{k_BT(q^2+\xi^{-2})}{\mu_V(\omega)}}. \quad (9)$$

Here, $S_\rho(\vec{q})$ is the static (charge) structure factor. Equations (8) and (9) determine $\mu_V(\omega)$ self-consistently, but we solve to leading order, replacing μ_V^{-1} in Eq. (9) by the zeroth order Γ_V. An approximate form is chosen for $S_\rho(\vec{q}) = \frac{k_BT\vec{q}^2}{2\pi n_0 e^2}\Theta(|\vec{q}_1| - |\vec{q}|) + \Theta(|\vec{q}| - |\vec{q}_1|)$ [n_0 being the total density of the charges and $|\vec{q}_1|$ a cutoff, corresponding to the first maximum in $S_\rho(\vec{q})$]. We find

$$\mu_V^{-1}(\omega) = \Gamma_V\left[1 + \frac{\pi J}{k_BT}\ln\left(1 + \frac{\vec{q}_1^2}{i\omega\Gamma_V + \xi^{-2}}\right)\right], \quad (10)$$

neglecting at first the second term of $S_\rho(\vec{q})$. The Coulomb-gas dielectric function of the system is related to the charge mobility μ_V and to the bound-pair part of the dielectric function by [10] $\varepsilon(\omega) = \varepsilon_B + ie^2 n_0 \mu_V(\omega)/\omega$.

We now present the results. Figure 1 shows, from Eq. (5), $\sigma_2/\sigma_0\xi^2$, as well as $\sigma_1/\sigma_0\xi^2$ (which for small ω is essentially $\mu_V^{-1}(\omega)$ the inverse vortex mobility, or vortex viscosity) versus the logarithmic scaled frequency or temperature variable, $\ln Y^{-1}$. The experimental data [4] have been obtained for field-induced free vortices [$\xi^{-1} = \xi_D^{-1}(f) \neq 0$] for which regime III is absent and $g(l) = [1 + (a/\xi)^2]^{-1}$, $\forall a$. Thus the coupling K_l should scale to zero for $l \to \infty$ (corresponding to $T > T_{KT}$ in the zero field case). We use the simple form $K_l = K_0\Theta(l_{max} - l)$, and use l_{max} as fitting parameter. A good fit is obtained for $l_{max} = 4.81$, which is on the order of the l value for which the linearized scaling equations [5] yield a vanishing K_l. $\sigma_1(\omega)$ clearly matches Drude behavior for regime I, $Y \gg 1$. The "intermediate" regime, $Y \lesssim 1$, with MP dependence $\sim \ln Y$ is seen to be fairly large. The experimental [4] data points for SNS arrays, shown in

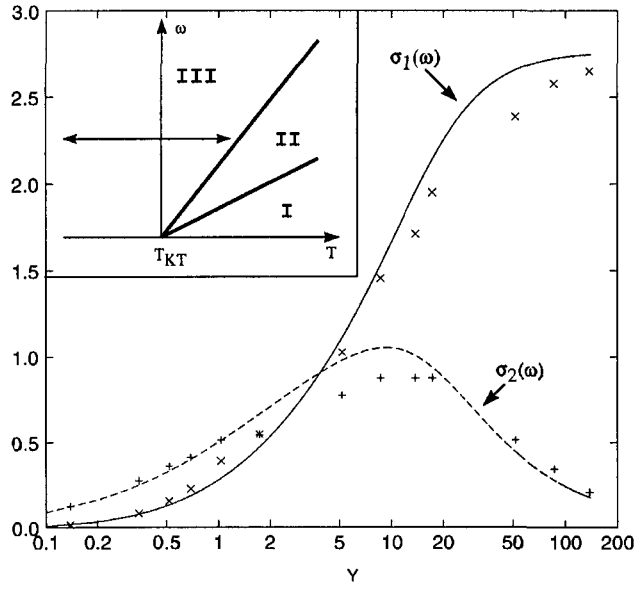

FIG. 1. Real and imaginary parts of the conductivity $\sigma/\sigma_0\xi^2$ versus $Y \equiv \Gamma_0/\omega\xi^2$, in a linear-log plot, from Eq. (5). Here ξ is the vortex screening length and $\sqrt{\Gamma_0/\omega}$ the probe length r_ω. The +, × symbols are experimental data points [4]. Inset: regimes I, II, and III in a schematic frequency-temperature diagram, with $r_\omega^{-1} = \xi_+^{-1}(T)$ defining the II/I boundary.

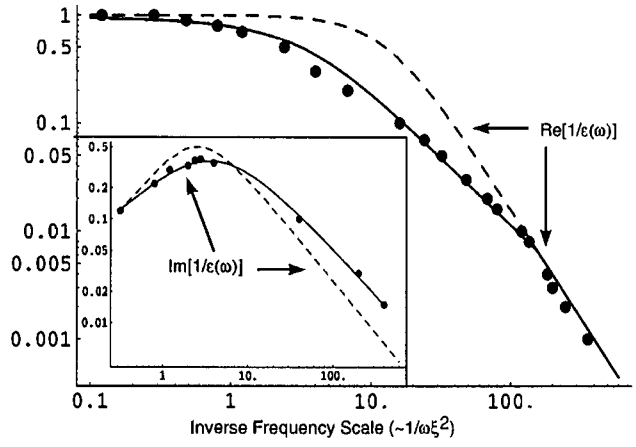

FIG. 2. Real and imaginary (inset) parts of $1/\varepsilon(\omega)$ versus an inverse frequency scale $\sim Y$, in a log-log plot. The constant-mobility $[\mu_V^{-1}(\omega) = \Gamma_V]$ Drude limit is represented by the dashed line, while the solid line is the result of our calculation (b). The experimental results of Ref. [4] are given by the dots.

Figs. 1 and 2, fall in regimes I and II. Very low frequency data are not unequivocal and are not shown. Typically [4], $\Gamma_0 \sim 300$ Hz, ω varies from ~ 10 Hz to ~ 10 kHz, for $R_J \sim 2\ \mathrm{m}\Omega$ (SNS arrays) and $I_J \sim 100$ nA, and $\xi(f) \sim 3.1$ for $f = 0.001$, so Y goes from ~ 0.1 to ~ 200.

Figure 2 shows the dielectric function $\varepsilon(\omega)$ [obtained through Eqs. (8) and (9), by using the full form of $S_\rho(\vec{p})$] as a function of Y. One again clearly recognizes two-frequency regimes (I and II), separated by a crossover frequency $\omega_{\mathrm{cross}} \approx (n_0\xi^2)^{-1}$. For $\omega > \omega_{\mathrm{cross}}$, $\Re(1/\varepsilon(\omega))$ varies like $|\omega|$ as in Minnhagen's regime II, whereas for $\omega < \omega_{\mathrm{cross}}$ it varies like ω^2, as in Drude's regime I. Moreover, we have verified for both methods that the ratio R_σ at $Y = 1$ varies between the Drude ($R_\sigma = 1$) and MP ($R_\sigma = 2/\pi$) signatures [7].

Regime III is not reached for the Y values shown in Fig. 1, but for SIS arrays, R_J is orders of magnitude higher, so the critical behavior might be more clearly seen. Below T_{KT}, or more generally, for $Y \ll 1$, one has effective damping coefficients $\eta_V \sim \sigma_1$ due to bound pairs, rather than free-vortex inverse mobilities, and $\sigma_1 \sim 1/\omega l_\omega^2$. This is consistent with simulations of driven vortices: there is a velocity-dependent viscosity coefficient, decreasing for larger velocities [16]. Larger oscillating pairs, probed at lower ω, are more sluggish, since they move in a logarithmically interacting viscous medium of smaller pairs.

In conclusion, we have proposed a regime interpretation of anomalous vortex dynamics, based on the ratio of the frequency-dependent probe scale, and the screening length. Both Drude and anomalous vortex dynamics emerge in different regimes, from calculations of the dynamic JJA conductivity and the vortex mobility. This reconciles different results, supports postulated conductivity scaling, and indicates further dynamical avenues to be explored, in simulations and experiments.

It is a pleasure to thank D. Bormann, P. Martinoli, and P. Minnhagen for useful conversations, and P. Martinoli for reading the manuscript.

[1] D. S. Fisher *et al.*, Phys. Rev. B **43**, 130 (1991).
[2] A. T. Dorsey, Phys. Rev. B **43**, 7575 (1991); A. T. Dorsey *et al.*, Phys. Rev. B **45**, 523 (1992).
[3] P. Minnhagen *et al.*, Phys. Rev. Lett. **74**, 3672 (1995).
[4] R. Théron *et al.*, Phys. Rev. Lett. **71**, 1246 (1993).
[5] J. M. Kosterlitz and D. J. Thouless, J. Phys. C **6**, 1181 (1973); **7**, 1046 (1974).
[6] Special issue on Coherence in Superconducting Networks, edited by J. E. Mooij and G. Schön [Physica (Amsterdam) **152B**, (1987)]; Special issue on Josephson Junction Arrays, edited by H. A. Cerdeira and S. R. Shenoy [Physica (Amsterdam) **222B** (1996)].
[7] H. Beck, M. Capezzali, and S. R. Shenoy (unpublished).
[8] V. Ambegaokar *et al.*, Phys. Rev. B **21**, 1806 (1980).
[9] S. R. Shenoy, J. Phys. C **18**, 5143, 5163 (1985); **20**, 2479 (1987).
[10] H. Beck, Phys. Rev. B **49**, 6153 (1994).
[11] P. Minnhagen, Rev. Mod. Phys. **59**, 1001 (1987); M. Wallin, Phys. Rev. B **41**, 6575 (1990); P. Minnhagen and O. Westman, Physica (Amsterdam) **320C**, 347 (1994); J. Houlrik *et al.*, Phys. Rev. B **50**, 3953 (1994).
[12] S. E. Korshunov, Phys. Rev. B **50**, 13 616 (1994).
[13] For SNS arrays, in addition to intergrain normal currents described by effective damping ν_0, there can be grain-to-substrate losses of normal current, incorporated in a generalized total current conserving dynamics as a local current term $(1/\nu_1)\dot{\theta}_i$ in Eq. (2). Here, the local damping rate ν_1 is scale independent. However, following the argument [9] through, there is, from the $(1/\nu_1)\dot{\theta}_i$ term, a decay rate in Fourier space $\nu_1 q^2$ that for q^{-1} in a, $a + da$ scales as ν_1/a^2, like $\nu_0 \rightarrow \nu_0/a^2$. Thus SIS ($\nu_0$ only) and SNS (ν_0, ν_1) arrays should have the same Coulomb-gas dynamics, as supported by calculation (b).
[14] K. K. Mon and S. Teitel, Phys. Rev. Lett. **62**, 673 (1989).
[15] W. Götze, Philos. Mag. B **43**, 219 (1981).
[16] T. Hagenaars *et al.*, Phys. Rev. B **50**, 1143 (1994).

ELSEVIER

Physica B 230–232 (1997) 962–965

PHYSICA B

Screening effects in superconductors

M. Capezzali[a,*], D. Ariosa[b], H. Beck[a]

[a] *Physics Department, University of Neuchâtel, Breguet 1,2000 Neuchâtel Switzerland*
[b] *IBM Research Division, Säumerstr. 4,8803 Rüschlikon (ZH), Switzerland*

Abstract

The partition function of the Hubbard model with local attraction and long-range Coulomb repulsion between electrons is written as a functional integral with an action A involving a pairing field Δ and a local potential V. After integration over V and over fluctuations in $|\Delta|^2$, the final form of A involves a Josephson coupling between the local phases of Δ and a "kinetic energy" term, representing the screened Coulomb interaction between charge fluctuations. The competition between Josephson coupling and charging energy allows to understand the relation between T_c and composition in high-T_c materials, in particular superlattices, alloys and bulk systems of low doping.

Keywords: Coulomb interaction; Phase diagram; Phase dynamics

We start with a Hamiltonian describing charge carriers (electrons or holes) on a lattice, subject to an on-site attraction, $-U$, and the long-range Coulomb repulsion, e^2V_C, acting on particles on different sites:

$$H = H_0 + H_U + H_C, \tag{1a}$$

$$H_0 = \sum_{\langle l,l'\rangle}\sum_{\sigma} t c^+_{l,\sigma}c_{l',\sigma} - \mu\sum_l N_l, \tag{1b}$$

$$H_U = -\frac{U}{2}\sum_{l,\sigma} c^+_{l,\sigma}c_{l,\sigma}c^+_{l,-\sigma}c_{l,-\sigma}, \tag{1c}$$

$$H_C = \frac{1}{2}\sum_{l\neq l'}(N_l - n_0)e^2V_C(l,l')(N_{l'} - n_0) \tag{1d}$$

Here $c^+_{l,\sigma}(c_{l,\sigma})$ are creation (annihilation) operators for charge carriers with spin σ at lattice site l, $\langle l,l'\rangle$ denotes pairs of nearest-neighbor sites, μ is the chemical potential, n_0 the background, neutralizing the density of charge carriers, and $N_l = \sum_\sigma c^+_{l,\sigma}c_{l,\sigma}$. The partition function can be written as a functional integral by means of two successive Stratonovich–Hubbard transformations [1, 2], decoupling the two interaction terms in H with the help of a complex field Δ and a real field V:

$$Z = \mathrm{Tr}\, e^{-\beta H} = \int D^2\Delta \int DV\, \mathrm{Tr}\, e^{-\beta H_0} \times T\exp\left\{-i\int_0^{-i\beta} d\tau\,[\tilde{H}(\Delta,V,\tau) + \varepsilon(\Delta,V,\tau)\right\}, \tag{2}$$

$$\tilde{H}(\Delta,V,\tau) = \sum_l [\Delta^*(l,\tau)c_{l,\uparrow}c_{l,\downarrow} + \mathrm{h.c.} + iV(l,\tau)(N_l(\tau) - n_0)], \tag{3a}$$

$$\varepsilon(\Delta,V,\tau) = \frac{1}{U}\sum_l |\Delta(l,\tau)^2| + \frac{1}{2e^2} \times \sum_{l\neq l'} V(l,\tau)V_C^{-1}(l,l')V(l',\tau). \tag{3b}$$

* Corresponding author.

PII S0921-4526(96)00712-0

We then evaluate the trace over the electronic degrees of freedom

$$\mathrm{Tr}\, e^{-\beta H_0}\, T\exp\left\{-i\int_0^{-i\beta} d\tau\,[\tilde{H}(\Delta,V,\tau) + \varepsilon(\Delta,V,\tau)]\right\} \equiv \exp\left\{-i\int_0^{i\beta} d\tau\, F(\Delta,V,\tau)\right\} \tag{4}$$

and we expand the "free energy" F up to fourth order in Δ and to second order in V and up to leading terms in space and time gradients of the two fields:

$$F = F_0 + F_{\Delta,V} \tag{5a}$$

$$F_{\Delta,V}(\tau) = \sum_l \left[a|\Delta(l,\tau)|^2 - id\Delta^*(l,\tau) \times\left(\frac{\partial}{\partial\tau} - 2V(l,\tau)\right)\Delta(l,\tau)\right] + c\sum_{\langle l,l'\rangle}|\Delta(l,\tau) - \Delta(l',\tau)|^2 + i\sum_l V(l,\tau)(\langle N_l\rangle - n_0) + \frac{1}{2e^2}\sum_{l,l'} V(l,\tau)V_{SC}^{-1}(l,l')V(l',\tau) + b\sum_l|\Delta(l,\tau)|^4. \tag{5b}$$

Here the coefficients a, b, c, d, are related to the free-electron particle–particle propagator [1–5], F_0 is the free-electron contribution, and $V_{SC}^{-1}(l,l') = V_C^{-1}(l,l') + \chi_0(l,l')$ is the screened Coulomb potential (approximated by its static limit) with $\chi_0(l,l')$ being the electronic polarizability. Integrating over the electric potential V yields

$$F_\Delta(\tau) = \sum_l\left[a|\Delta(l,\tau)|^2 + b|\Delta(l,\tau)|^4 - id\Delta^*(l,\tau)\frac{\partial\Delta(l,\tau)}{\partial\tau}\right] + c\sum_{\langle l,l'\rangle}|\Delta(l,\tau) - \Delta(l',\tau)|^2 + \frac{1}{2e^2}\sum_{l,l'}\rho(l,\tau)V_{SC}(l,l')\rho(l',\tau), \tag{6}$$

where $\rho(l,\tau) = 2d|\Delta(l,\tau)|^2 + \langle N_l\rangle - n_0$ represents charge density fluctuations. Next we introduce amplitude and phase of Δ. In the following, we assume to be in a relatively strong coupling regime ($t \ll U$) in which fermions bind into on-site singlet pairs at a temperature of the order of the mean field transition temperature T_{mf}, well above the superconducting phase transition, the latter being finally triggered by the onset of phase order [6–8]. Below T_{mf}, $a < 0$, so that the average amplitude has a non-vanishing mean value Δ_0 given by $a + 2b\Delta_0^2 = 0$. Charge neutrality implies $2d\Delta_0^2 + \langle N_l\rangle - n_0 = 0$ and, for $t \ll U$[1, 3–5, 9]:

$$c = \frac{2t^2}{U^3}, \qquad d = \frac{1}{U^2}, \tag{7a}$$

$$\Delta_0^2 = \tfrac{1}{4}n_0(2 - n_0)U^2 \approx \tfrac{1}{2}n_0U^2 \quad \text{for } n_0 \ll 1. \tag{7b}$$

Splitting the number of pairs at a given site into $|\Delta(l,\tau)|^2 = \Delta_0^2 + \frac{1}{2}U^2\delta n_p(l,\tau)$, we integrate over $\delta n_p(l,\tau)$ which (neglecting gradient terms) yields a free energy functional for phase fluctuations only:

$$F_\Theta(\tau) = J\sum_{\langle l,l'\rangle}[1 - \cos(\Theta(l,\tau) - \Theta(l',\tau))] + \frac{n_0}{2}\sum_l\frac{\partial\Theta(l,\tau)}{\partial\tau} - \frac{1}{2}\sum_{l,l'}\frac{\partial\Theta(l,\tau)}{\partial\tau} \times\frac{1}{(2e)^2}W^{-1}(l,l')\frac{\partial\Theta(l',\tau)}{\partial\tau} \tag{8a}$$

with the Josephson coupling [1, 9] $J = 2c\Delta_0^2 = 2n_0(t^2/U)$, and

$$W(l,l') = \begin{cases} V_{SC}(l,l'), & l\neq l', \\ (2e)^2 b/d^2, & l = l' \end{cases} \tag{8b}$$

Our expansion of F in powers of Δ has yielded the on-site repulsion $(2e)^2b/d^2$ between pairs. However, due to the exclusion principle, two pairs cannot really sit on the same lattice site. Thus, in the following, we exclude $l = l'$ in the last term of (8a). By going from the "phase velocities" $(\partial\Theta(l,\tau)/\partial\tau)$ to the conjugate momenta $p(l,\tau)$ we end up with the partition function of the Hamiltonian [10]

$$H = \frac{1}{2}\sum_{l,l'}\left(p(l) - \frac{n_0}{2}\right)[(2e)^2W(l,l')] \times\left(p(l') - \frac{n_0}{2}\right) + J\sum_{\langle l,l'\rangle}[1 - \cos(\Theta(l) - \Theta(l'))]. \tag{9}$$

Hamiltonian (9) describes the relevant physics of short coherence length superconductors in terms of Josephson coupled spatial phase variations and "charge fluctuations" coupled by the screened Coulomb interaction. It is also the "phase-only" representation of the Hamiltonian of interacting bosons [10–12]. Its critical behavior, in particular the influence of the "background", $-\frac{1}{2}n_0$, has been studied in these references. Here, we apply expression (9) to calculate the transition temperature of strongly anisotropic superconductors, such as superlattices and bulk systems in the underdoped regime [13]. We make the following approximations: (i) H is restricted to one superconducting layer; (ii) the screened Coulomb interaction, which takes into account the electric coupling between layers, is modelled by a Yukawa-form, with a Thomas–Fermi screening length λ_{TF}, depending on the density n_0 of charge carriers according to the well-known formula

$$\lambda_{TF}^{-1} = \frac{1}{2\pi}\frac{2.95}{\sqrt{r_s/a_0}}\,[\text{Å}^{-1}],$$

where $r_s = (3/(4\pi n_0))^{1/3}$ and a_0 is the Bohr radius; (iii) considering only $n_0 \ll 1$, the "background shift", $-\frac{1}{2}n_0$, in the first term of (9) is neglected. We make connection with previous work [14, 15] by mapping (9) onto a "capacity model":

$$\frac{1}{2}\sum_{l,l'} p(l)[(2e)^2 W(l,l')]p(l') \approx \frac{(2e)^2}{2C}\sum_l p(l)^2, \qquad (10)$$

with

$$\frac{1}{2C} = \frac{1}{e^2}\sum_{l=0} W(l,0) = \frac{2\pi\lambda_{TF}}{\varepsilon a_L^2}\,e^{-a_L/\lambda_{TF}}.$$

This is the XY-model with kinetic energy [14, 15], ε being the dielectric constant of the interlayer material and a_L the lattice constant. In Ref. [14] the critical temperature in two dimensions was evaluated in the "self-consistent harmonic approximation" (SCHA) which gives results in good agreement with Monte Carlo simulations [16]. A good overall fit of the numerical SCHA result is [17] $T_C(\alpha) \approx T_C(0)\sqrt{1-\alpha/\alpha_C}$ where $\alpha = (2e)^2/(2CJ)$ is the ratio between charging and Josephson energy. When α approches $\alpha_C = 6.2$, T_C goes to zero. This approach has been successfully applied [14, 15] to calculating the superconducting transition temperature for superlattices and for alloys by determining the appropriate effective capacity through electrostatic considerations.

We finally use Hamiltonian (9) to find T_C as a function of doping for high-T_C superconductors in the underdoped regime. For $YBa_2Cu_3O_7$, our "capacity model" has allowed to fit the T_C variation of both, superlattices and alloys, in a coherent way, using SCHA [14, 15] for $J = 120$ K at optimal doping ($n_0 \approx 0.16$ of holes per cell [13]). Below optimal doping, the ratio α increases when the number n_0 of charge carriers is reduced: the n_0 dependence of J is given following Eq. (8a) and C varies with n_0 through the screening length λ_{TF}. Using the above expression for $T_C(\alpha)$, with doping-dependent J and C, we then find that T_C should be zero for $n_0 \approx 0.07$, in good agreement with the measured phase diagram [13]. This shows that the phase boundary in the underdoped regime can be understood in terms of Bose–Einstein condensation of preformed pairs, T_C being suppressed by phase fluctuations when the minimum doping is approached.

In summary, starting from the attractive Hubbard model with long-range Coulomb repulsion, we have given a microscopic derivation of a description of short coherence length superconductors in terms of the superconducting phase, the Hamiltonian for which includes a "charging energy" and a Josephson coupling. This is a microscopic justification of such a Hamiltonian, which has been used previously [14, 15] in calculating T_C for superlattices and alloys and also allows understanding the phase boundary of bulk oxides in the underdoped regime.

This work was supported by the Swiss National Science Foundation. We thank T. Schneider and M.H. Pedersen for valuable discussions.

References

[1] T.K. Kopec and H. Umezawa, Phys. Rev. B 47 (1993) 8923.
[2] V. Ambegaokar, U. Eckern and G. Schön, Phys. Rev. Lett. 46 (1982) 211.
[3] M. Drechsler and W. Zwerger, Ann. Phys. 1 (1992) 15.

[4] M. Randeria, in: "Bose–Einstein Condensation", eds. A. Griffin, D. Snoke and S.S. Tringari (Cambridge University Press, Cambridge, 1994).
[5] M.H. Pedersen and H. Beck, unpublished.
[6] V.J. Emery and S.A. Kivelson, Nature 374 (1995) 434, Phys. Rev. Lett. 74 (1995) 3253.
[7] S. Doniach and M. Inui, Phys. Rev. B 41 (1990) 6668.
[8] E. Roddick and D. Stroud, Phys. Rev. Lett. 74 (1995) 1430.
[9] J.J. Vicente Alvarez and C.A. Balseiro, Solid State Commun. 98 (1996) 313.
[10] M.P.A. Fisher and G. Grinstein, Phys. Rev. Lett. 60 (1988) 208.
[11] Min-Chul Cha and S.M. Girvin, Phys. Rev. B 49 (1994) 9794.
[12] M.P.A. Fisher, P.B. Weichmann, G. Grinstein and D.S. Fisher, Phys. Rev. B 40 (1989) 546; A. van Otterlo, K.H. Wagenblast, R. Baltin, C. Bruder, R. Fazio and G. Schön, Phys. Rev. B 52 (1995) 16 176.
[13] J.L. Tallon and N.E. Flower, Physica C 204 (1993) 237.
[14] D. Ariosa and H. Beck, Phys Rev B 43 (1991) 344.
[15] D. Ariosa, T. Luthy, V. Tsaneva, B. Jeanneret, H. Beck and P.Martinoli, Physica B 194–196 (1994) 2371.
[16] L. Jacobs, J.V. Jose, M.A. Novotny and A.M. Goldman, Phys. Rev. B 38 (1988) 4562.
[17] D. Ariosa, J. Perret, H. Beck and P. Martinoli, in preparation.

PHYSICAL REVIEW B VOLUME 57, NUMBER 10 1 MARCH 1998-II

One-electron spectral functions of the attractive Hubbard model for intermediate coupling

Maxim Yu. Kagan
P.L. Kapitza Institute for Physical Problems, Kosygin Str. 2, 117334 Moscow, Russian Federation

Raymond Frésard, Massimiliano Capezzali, and Hans Beck
Institut de Physique, Université de Neuchâtel, Rue A.L. Breguet 1, 2000 Neuchâtel, Switzerland
(Received 9 April 1997)

We calculate the one-electron spectral function of the attractive (negative-U) Hubbard model. We work in the intermediate-coupling and low-density regime and obtain the self-energy in an approximate analytical form. The excitation spectrum is found to consist of three branches. The results are obtained in a framework based on the self-consistent T-matrix approximation, which is compatible with the Mermin-Wagner theorem. [S0163-1829(98)09309-6]

I. INTRODUCTION

The Hubbard model involving electrons on a lattice, subject to an attractive interaction when they are on the same site, is one of the simplest models for describing superconductivity. Despite its simplicity, it has turned out to be very challenging for the theoreticians to give a simple description of its properties which is valid in the various regimes of coupling strength. In the weak-coupling regime, the link with BCS theory of superconductivity has been done by Nozières and Schmitt-Rink.[1] At sufficiently low T, an instability of the Fermi sea towards superconductivity occurs. In three dimensions, the transition is essentially mean-field in character. In the opposite strong-coupling limit ($|U|\to\infty$), the electrons form bound pairs which are immobile since they can only move via virtual ionization with an infinite energy barrier. However, for large but finite U, those bound pairs essentially behave like heavy hard-core bosons [with an effective mass $m^*\sim m(U/t)$] which are undergoing Bose-Einstein condensation at sufficiently low T. On the lattice, T_C vanishes in the limit $|U|\to\infty$, while in the continuum limit, it remains finite.[2] This difference is due to the absence of a pair-hopping term when working on the lattice.

In the intermediate-coupling regime, the physics will be dominated by the interplay between the quasiparticles and the bound pairs, which may lead to nontrivial behavior. Some basic physical features characterizing this regime have been previously studied by numerical means,[3] which showed important deviations from canonical Fermi-liquid theory.

Even though it is still lacking a microscopical derivation, the attractive Hubbard model is interesting in its own right, since it allows for studying various routes leading to superconductivity. Since the interaction is local, it will be s-wave superconductivity, but the generalization to nonlocal interaction can be considered.[4] In the weak-coupling regime, perturbation theory is expected to work, and this has been worked out by a series of authors,[5] some of them focusing on two-dimensional (2D) systems.[6] Of special interest is the low-density regime where chances of obtaining meaningful results are better, since the ratio of the scattering length to the average interparticle distance can be used as a small parameter. Unfortunately those calculations are quickly becoming very involved since the simplest conserving approximation is the self-consistent T-matrix approach.[7–9] Alternatively, variational-Monte Carlo calculations, based on the Gutzwiller wave-function[10] and quantum Monte Carlo (QMC) simulations have been performed.[11] These methods are providing results which then generate a need for a qualitative analytical understanding. To that aim simpler calculations based on Hubbard-Stratonovitch decoupling of the interaction,[12] slave-boson mean-field calculations (see, for instance, Ref. 13, and references therein), or on the moment calculation of the electronic spectral function have been performed.[14] Unfortunately the latter does not account for the damping of the quasiparticles.

The aim of this paper is to treat analytically the intermediate-coupling regime, which is the most delicate. This allows us to give an analytical account of the results obtained with QMC simulations. We first review the self-consistent T-matrix approximation. As pointed out by several authors,[15] the corresponding numerical calculations typically yield a superconducting instability at a finite T, even in two dimensions. This contradicts the Mermin-Wagner theorem. We then propose an alternative scheme which complies with this theorem. We then proceed to the calculation of the electronic structure.

II. THEORETICAL FRAMEWORK

We study the Hubbard model on the square lattice:

$$H=\sum_{i,j}\sum_{\langle\sigma\rangle} t_{ij}c^{\dagger}_{i,\sigma}c_{j,\sigma}+U\sum_{i} n_{i,\uparrow}n_{i,\downarrow}. \tag{1}$$

We consider an attractive interaction ($U<0$) in the intermediate-coupling regime ($|U|\lesssim W$), W being the bandwidth. In two dimensions, any attractive potential has a bound state. In the case $|U|=W$, the binding energy E_b has been found to be $E_b\approx 0.2W$,[8] namely $E_b\ll W$. We are thus in a situation where bound pairs exist and have a strong influence on the physics via the splitting of the noninteracting band into two subbands. In this regime, the pairs are extended. They become purely local only in the $|U|=\infty$ limit, since for any finite U they can move via virtual ionization.[1]

We also note that the BCS theory successfully describes the weak-coupling regime. However there does not exist any analytical theory in the intermediate-coupling regime, and most results are obtained out of numerical simulations.[6,11] In the low-density regime, the self-consistent T-matrix approximation is expected to be exact and has been solved by a variety of authors.[7–9] Unfortunately, numerical difficulties prevented those authors from obtaining results for arbitrary U. We also note that the numerical solutions may lead to unphysical results such as a finite critical temperature for Bose condensation of the pairs in two dimensions, which is contradicting the Mermin-Wagner theorem. We believe (see below) that this is due to the use of an inappropriate expression for the particle density. That however does not discredit the scheme, and we are basing our approach on it. It amounts to solving

$$T(\vec{q},i\nu_n)=\frac{-U}{1+U\chi(\vec{q},i\nu_n)}, \tag{2}$$

$$\chi(\vec{q},i\nu_n)=\beta^{-1}\sum_{\vec{p},i\omega_n} G(\vec{p},i\omega_n)G(\vec{q}-\vec{p},i\nu_n-i\omega_n), \tag{3}$$

$$\Sigma(\vec{q},i\omega_n)=-\beta^{-1}\sum_{\vec{p},i\nu_n} T(\vec{p},i\nu_n)G(\vec{p}-\vec{q},i\nu_n-i\omega_n), \tag{4}$$

$$G(\vec{q},i\omega_n)=\frac{1}{i\omega_n-t_{\vec{q}}+\mu-\Sigma(\vec{q},i\omega_n)}. \tag{5}$$

Here, ω_n are fermionic, and ν_n bosonic Matsubara frequencies, while $t_{\vec{q}}$ represents the (eventually renormalized) kinetic energy. This set of equations is valid *above* T_c, as no anomalous Green's function enters. Otherwise one can resort to the scheme obtained by Pedersen *et al.*, by functional derivative techniques.[12] This approximation is conserving and it diagrammatically corresponds to summing up the dressed particle-particle ladder which includes the leading order in an expansion in $k_F a$.[5,9] Another important quantity is the two-particle Green's function which is defined by

$$G^{(2)}(\vec{q},i\nu_n)=\int_0^\beta e^{i\nu_n\tau}\langle T_\tau[Q(\vec{q},\tau)Q^\dagger(-\vec{q},0)]\rangle d\tau, \tag{6}$$

where T_τ is the usual time-ordering operator and the operator

$$Q^+(\vec{q})=\frac{1}{N}\sum_{\vec{k}} c^\dagger_{-\vec{k},\uparrow}c^\dagger_{\vec{k}-\vec{q},\downarrow} \tag{7}$$

creates a pair having (center-of-mass) wave vector $\vec{q}$. $G^{(2)}(\vec{q},i\nu_n)$ is related to the T-matrix by

$$G^{(2)}(\vec{q},i\nu_n)=\frac{U+T(\vec{q},i\nu_n)}{U^2}. \tag{8}$$

We calculate $G^{(2)}(\vec{q},i\nu_n)$ by inserting the free-electron Green's function into expression (3) for $\chi(\vec{q},i\nu_n)$. For simplicity, we approximate the density of states (DOS), $\rho(\epsilon)$, of the tight-binding band resulting from the Hamiltonian (1) by the square DOS [i.e., $\rho(\epsilon)=1/W$ for $|\epsilon|\leq W/2$ and $\rho(\epsilon)=0$ otherwise].

For small momenta, $G^{(2)}(\vec{q},i\nu_n)$ is given by

$$G^{(2)}(\vec{q},i\nu_n)=\frac{1}{2W(1-q^2/16)}\frac{\ln\left\{\dfrac{[i\nu_n+\mu_B-|E_b|-2W+(q^2t/2)]}{[i\nu_n+\mu_B-|E_b|-q^2t/2]}\right\}\ln\Phi}{\ln\Phi-\left(1+\dfrac{q^2}{16}\right)\ln\left\{\dfrac{[i\nu_n+\mu_B-|E_b|-2W+(q^2t/2)]}{[i\nu_n+\mu_B-|E_b|-(q^2t/2)]}\right\}}, \tag{9}$$

where $\mu_B=2\mu+W+|E_b|$, $\Phi=(2W+|E_b|)/|E_b|$ and $|E_b|$ is the binding energy of a pair. The binding energy is obtained as a solution of

$$-\frac{1}{U}=\chi(\vec{q}=\vec{0},\omega=E_b)|_{\mu=-W/2}, \tag{10}$$

which yields

$$|E_b|=2W\left(\frac{1}{e^{-2W/U}-1}\right). \tag{11}$$

The form (9) has the correct behavior for ν_n going to infinity in the low-density regime, i.e., $G^{(2)}(\vec{q},i\nu_n)\to 1/i\nu_n$.

The spectrum of $G^{(2)}(\vec{q},i\nu_n)$ presents two features: (i) a sharp quasiparticle peak, which can be found by expanding Eq. (9) with respect to $i\nu_n+\mu_B-q^2t/2$; (ii) a continuous spectrum which extends over energies above the one of the quasiparticle. Correspondingly, the lowest order form of the T matrix, valid for small wave vector and frequency is given by

$$T_0(\vec{q},i\nu_n)=\frac{-|E_b|^2\Phi}{i\nu_n-\vec{q}^2/4m_0^*+\mu_B}. \tag{12}$$

The mass renormalization factor of a pair is given by

$$Z\equiv\frac{m}{m_0^*}=\frac{W+|E_b|}{W}-\frac{|E_b|^2}{2W^2}\Phi\ln\Phi. \tag{13}$$

In the intermediate-coupling regime, the mass is only weakly renormalized while in the strong-coupling regime, there is a strong renormalization of the order $W/|U|$. Due to the relationship between the two-particle T matrix and the two-

particle Green's function, the quantity μ_B that we defined above does represent the chemical potential of a pair, which has bosonic character.

For $\vec{q}$'s close to the nesting vector $\vec{Q}=(\pi,\pi)$, we obtain

$$T_0(\vec{q},i\nu_n)=\frac{-U^2}{i\nu_n+(\vec{q}-\vec{Q})^2/4m^*+2\mu+|U|}. \quad (14)$$

In the vicinity of the zone corner, the renormalization of the pair mass is different from the one close to the zone center. Even in the intermediate-coupling regime, it is strongly renormalized to be $m^*/m\approx|U|/t$. At $\vec{q}=\vec{Q}$, the form (9) of the T matrix is actually exact, related to the fact that the creation operator

$$\eta^\dagger=\sum_{\vec{p}} c^\dagger_{\vec{p}+\vec{Q},\uparrow}c^\dagger_{-\vec{p},\downarrow} \quad (15)$$

of an "η pair" with center-of-mass momentum $\vec{Q}$, satisfies the simple commutation relation:[16–18]

$$[H,\eta^\dagger]=(U-2\mu)\eta^\dagger. \quad (16)$$

Using the above expressions (12) and (14), we can calculate the self-energy. To lowest order, we insert the free-electron Green's function in Eq. (4). The first contribution to the self-energy arises from the poles of the T matrix. Due to the statistical factors we obtain (to that order of approximation) that the contribution of the η resonance is exponentially small, as well as those following from the poles of the Green's function. After performing analytical continuation, we are left with

$$\Sigma_1(\vec{k},\omega)=\frac{U^2n_d}{\omega+t_{\vec{k}}-\mu+\mu_B+i0^+}. \quad (17)$$

The quantity n_d will be defined below, in Eqs. (26) and (27). $\Sigma_1(\vec{k},\omega)$ yields then the Green's function as

$$G(\vec{k},\omega)=\frac{1}{2}\left(1+\frac{2(t_{\vec{k}}-\mu)-\mu_B}{x_{\vec{k}}}\right)\frac{1}{\omega+\frac{1}{2}\mu_B-\frac{1}{2}x_{\vec{k}}+i0^+}+\frac{1}{2}\left(1-\frac{2(t_{\vec{k}}-\mu)+\mu_B}{x_{\vec{k}}}\right)\frac{1}{\omega+\frac{1}{2}\mu_B+\frac{1}{2}x_{\vec{k}}+i0^+}, \quad (18)$$

where $x_{\vec{k}}=\sqrt{[2(t_{\vec{k}}-\mu)+\mu_B]^2+4U^2n_d}$. We immediately note the two limiting behaviors, with respect to momentum $\vec{k}$:

$$x_{\vec{k}}\approx\Delta+2t\gamma k^2, \quad (19)$$

with $\gamma=|E_b|/\Delta$ and

$$\Delta=\sqrt{|E_b|^2+4U^2n_d} \quad (20)$$

for small momenta; respectively,

$$x_{\vec{k}}\approx 2(t_{\vec{k}}-\mu)+\mu_B+\frac{2U^2n_d}{2(t_{\vec{k}}-\mu)+\mu_B}, \quad (21)$$

for large momenta.

At this stage of the calculation, the Green's function has a two-pole structure. The lower excitation branch corresponds to quasibound fermions (hereafter denoted as "bosonic" band), while the upper branch describes the unpaired fermions (fermionic band). At small momenta, we obtain

$$G(\vec{k},\omega)=\frac{\Delta+|E_b|}{2\Delta}\frac{1}{\omega+1/2(\mu_B-\Delta)-\gamma tk^2+i0^+}+\frac{\Delta-|E_b|}{2\Delta}\frac{1}{\omega+1/2(\mu_B+\Delta)+\gamma tk^2+i0^+} \quad (22)$$

with the spectral weight mainly located in the unpaired fermion band [first contribution in Eq. (22)]. At large momenta, the Green's function results into

$$G(\vec{k},\omega)=\frac{1-2U^2n_d/[2(t_{\vec{k}}-\mu)+\mu_B]^2}{\omega-(t_{\vec{k}}-\mu)+i0^+}+\frac{2U^2n_d/[2(t_{\vec{k}}-\mu)+\mu_B]^2}{\omega+t_{\vec{k}}-\mu+\mu_B+i0^+}, \quad (23)$$

where the weight of the paired fermion band is even smaller than for small momenta. The form of the Green's function Eq. (18) differs from the one of Ref. 20 because the chemical potential μ is located below the fermionic band in our problem.

We note that there are two equivalent expressions for the particle density operator $\hat{n}$:

$$\hat{n}_i=\sum_\sigma[\hat{n}_{i,\sigma}(1-\hat{n}_{i,-\sigma})+\hat{n}_{i,\sigma}\hat{n}_{i,-\sigma}]. \quad (24)$$

On one hand, we can use the left-hand side to express the particle density n as n_1, where the subscript 1 indicates that the density is calculated out of the one-particle Green's function:

$$n_1=\beta^{-1}\sum_{i\omega_n,\vec{k}}\sum_\sigma G_\sigma(\vec{k},i\omega_n)e^{i\omega_n 0^+}. \quad (25)$$

Alternatively, we may use the right-hand side (rhs) of Eq. (24) by separating explicitly the contributions from the unpaired fermions (first term) and the doubly occupied sites (second term). The total density n_d of the latter is given by

$$n_d=\frac{1}{\beta}\sum_{\vec{q}}\sum_{i\nu_n}G^{(2)}(\vec{q},i\nu_n)e^{i\nu_n 0^+}=\sum_{\vec{q}}\int_{-\infty}^{\infty}\frac{d\omega}{2\pi}\mathrm{Im}\{G^{(2)}(\vec{q},\omega+i0^+)\}N_B(\omega), \quad (26)$$

$N_B(\omega)$ being the Bose-Einstein distribution function. Owing to the latter, at low temperatures, only the low-energy part of the two-particle spectrum, $\mathrm{Im}\{G^{(2)}(\vec{q},\omega+i0^+)\}$, will con-

tribute to n_d. According to the discussion following Eq. (11), this low-energy part has two contributions: the sharp quasiparticle excitation, given by Eq. (12), which dominates for small momenta, and the low-frequency tail of the continuous spectrum of $G^{(2)}(\vec{q},i\nu_n)$. Since it does not have a sharp structure, it would only contribute a featureless background to the one-electron spectral function; thus, we have neglected it for the calculation of the self-energy $\Sigma_1(\vec{k},\omega)$. Neglecting the continuum also in calculating n_d, we find, according to Eqs. (8), (12), and (26):

$$n_d = R\sum_{\vec{q}} N_B\left(\frac{q^2}{4m}Z-\mu_B\right). \tag{27}$$

Thus, in our approximation, the number of doubly occupied sites n_d is given by the "number of bosons," n_B

$$n_B \equiv \sum_{q} N_B\left(\frac{q^2}{4m}Z-\mu_B\right), \tag{28}$$

weighted by a factor

$$R=\left(\frac{|E_b|}{2W}\right)^2 \Phi(\ln\Phi)^2, \tag{29}$$

which is the residue of the two-particle Green's function at the bottom of the two-particle band. These bosons, having energy $E_B=(q^2/4m)Z$ and chemical potential μ_B, represent pairs of electrons being (virtually) bound by the on-site attraction. These results correspond to the observation of other authors (see, for example, Ref. 9) that, for sufficiently strong attraction, the two-particle Green's function, (respectively, the T matrix) can be interpreted as a "bosonic Green's function." However, there is a weight factor between the two. For large $|U|$, this weight factor R goes to one: in the strong-coupling limit, all the double occupancy is due to coherently propagating quasibound pairs. In the intermediate-coupling regime, which we want to consider ($|U|\lesssim W$), the weight factor R is roughly 0.5: only about one half of the two-particle spectrum in Eq. (9) is resulting from coherent excitations. In the weak-coupling regime, R vanishes, thus rendering our approximation invalid in this limit.

Since, in our approach, there is gap in the one-electron spectrum, separating the "bosonic" band from the fermionic one, there is no difficulty in obtaining the number of unpaired electrons n_F as

$$n_F=\sum_{\vec{k},\sigma} \Xi_{\vec{k}} f_F(\varepsilon_{\vec{k},\sigma}), \tag{30}$$

where $f_F(\varepsilon_{\vec{k},\sigma})$ is the usual Fermi distribution function. The dispersion $\varepsilon_{\vec{k},\sigma}$ of the unpaired fermions and the spectral weight $\Xi_{\vec{k}}$ entering Eq. (30) are

$$\varepsilon_{\vec{k},\sigma}=\frac{1}{2}(x_{\vec{k}}-\mu_B),$$

$$\Xi_{\vec{k}}=\frac{1}{2}\left(1+\frac{2(t_{\vec{k}}-\mu)-\mu_B}{x_{\vec{k}}}\right). \tag{31}$$

The total particle density results into

$$n=n_F+2n_d. \tag{32}$$

For noninteracting particles, we may equally well use both rhs and lhs of Eq. (24) to calculate the density, since Wick's theorem applies. However, the identity (24) may be violated in an approximate treatment like perturbation theory. This is the reason why the self-consistent T-matrix calculation breaks down at low T in two dimensions. By calculating the density by means of Eq. (25), there is nothing preventing $T(\vec{q}=\vec{0},\omega=0)$ from diverging at finite T, signaling a phase transition, while using Eq. (32) would definitively keep $T(\vec{0},0)$ finite for any finite temperature. By making use of Eq. (32), we make sure that Bose condensation can only take place at $T=0$, in agreement with the Mermin-Wagner theorem. Indeed, according to the expressions (27) and (28) for n_d and n_B, respectively, the bosonic chemical potential μ_B, for a given n_d (or n_B) and for $d=2$, is different from zero at any finite temperature, which inhibits Bose condensation, except for $T=0$. In principle, for $d=2$ one should see a Kosterlitz-Thouless (KT) transition. However, since our approximation does not treat the bosonic phase fluctuations in an adequate way, we cannot expect to see the KT scenario. On the other hand, T_c may well be finite for a 3D system. Actually our procedure is similar in spirit to the two-particle self-consistent approach to the repulsive Hubbard model by Vilk *et al.*[19,20]

Now for a two-dimensional system, we can explicitly evaluate the number of pairs. We obtain

$$n_d=\frac{2R}{\beta WZ}\ln\left(\frac{e^{-\beta[W(Z/2)-\mu_B]}-1}{e^{\beta\mu_B}-1}\right), \tag{33}$$

$$n_F=\frac{1}{\beta W\gamma}\left(\frac{|E_b|+\Delta}{\Delta}\right)\ln\left(\frac{e^{\beta/2(\mu_B-\Delta)}+1}{e^{\beta/2(\mu_B-\Delta-\gamma W)}+1}\right), \tag{34}$$

where Δ and γ have been given above.

After having carefully chosen the density n (see below), we are ready to (numerically) solve Eqs. (32), (33), and (34) for the chemical potential, as a function of temperature. The resulting $\mu_B(T)$ vanishes exponentially at $T=0$. From Eqs. (8) and (12), we obtain that the range of the two-particle Green's function ξ is given by

$$\frac{\xi}{a}=\sqrt{\frac{t}{2|\mu_B|}}, \tag{35}$$

where a is the lattice spacing. It is displayed in Fig. 1, for three different values of the coupling strength U and with fixed density $n=0.1$. We note that it shows a strong dependence on U. At very low temperatures, it is given by

$$\frac{\xi}{a}=\sqrt{\frac{\beta t}{2}}e^{\beta WZn/8R}. \tag{36}$$

Oppositely, in the intermediate temperature range, ξ becomes independent of U. We also find that ξ decreases with increasing $|U|$. In the strong-coupling limit the ratio Z/R tends to zero and thus the exponential divergence of ξ in $1/T$ is suppressed (there remains only the power-law dependence $\xi\sim 1/\sqrt{T}$).

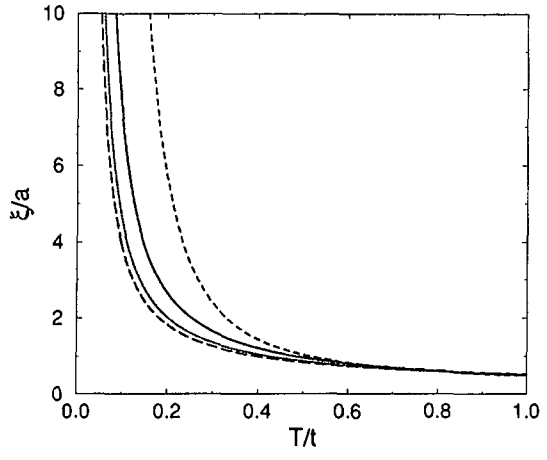

FIG. 1. Range of the two-particle Green's function, as a function of temperature T, at density $n=0.1$, for three different interaction strengths, $U=-4t$ (short-dashed line), $U=-6t$ (full line), $U=-8t$ (dotted line), and $U=-10t$ (long-dashed line).

We may now define a coherence temperature $T_{\rm coh}$ as the temperature at which the range of the two-particle Green's function exceeds 10 lattice spacings. We obtain $T_{\rm coh}\approx 0.16t$ for $U=-4t$ and $T_{\rm coh}\approx 0.1t$ for $U=-6t$, which may be compared to T_c as obtained from the numerical simulations.[11] We see that they compare favorably and that, moreover, $T_{\rm coh}$ decreases with increasing U, again in agreement with numerical simulations. Finally, we note that ξ becomes of the order of the lattice spacing at temperatures well below $|E_b|/2$. We now turn to the temperature dependence of the number of pairs. It is displayed in Fig. 2, as a function of T, for three different values of U and at density $n=0.04$. At low temperatures, it is independent of T. Since the binding energy of the pair (and the gap) decreases as U gets smaller, n_d begins to decrease at a lower T for $U=-6t$ than for $U=-10t$, for example. In all cases n_d decreases by a factor 2 at $T\approx\Delta/2$.

In order to reach a better self-consistency, we now calculate how the quasibound states affect the two-particle propagator. Our approach is perturbative, in the sense that we want

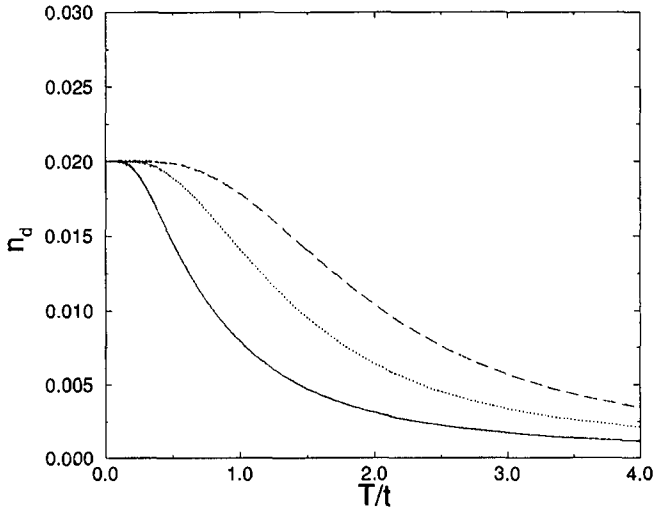

FIG. 2. Density of quasibound pairs as a function of temperature T, at density $n=0.04$, for $U=-6t$ (full line), $U=-8t$ (dotted line), and $U=-10t$ (dashed line).

to obtain the correction to the self-energy [which will be denoted below as $\Sigma_2(\vec{q},i\omega_n)$] after having performed the first iteration of the Eq. (4), which results into the Green's function given by Eq. (18). The task can be performed analytically provided that the upper fermionic branch in Eq. (18) and the unperturbed initial Green's function $G_0(\vec{q},i\omega_n)$ almost cancel each other (i.e., present comparable weights and denominators). This imposes a precise limitation on the choice of the two parameters of our model, i.e., the coupling strength U and the density n. It reads

$$\frac{\Delta-E_b}{2\Delta}\ll 1. \tag{37}$$

In this regime, we may consider only the lower (bosonic) branch of the Green's function, given by Eq. (18); hereafter, it will be denoted as $G_1(\vec{q},i\omega_n)$. This is an important point to stress; although the bosonic branch has a very small spectral weight, it contains the most important physics in the low-density limit, at least at the level of the perturbative approach we have adopted. We calculate the first correction to the two-particle propagator as χ_1, with

$$\chi_1(\vec{q},i\nu_n)=\sum_{i\omega_n,\vec{p}} G_1(\vec{q}-\vec{p},i\nu_n-i\omega_n)G_0(\vec{p},i\omega_n) + \sum_{i\omega_n,\vec{p}} G_0(\vec{q}-\vec{p},i\nu_n-i\omega_n)G_1(\vec{p},i\omega_n). \tag{38}$$

Carrying out the summation over Matsubara frequencies, we obtain that the statistical factors are exponentially small and thus there is no correction to χ to that order. Thus, the T matrix is still given by Eq. (12). We can now proceed to the calculation of the second-order correction to the self-energy. It is given by

$$\Sigma_2(\vec{q},i\omega_n)=\sum_{i\nu_n,\vec{p}} T_0(\vec{p},i\nu_n)G_1(\vec{p}+\vec{q},i\nu_n+i\omega_n), \tag{39}$$

yielding, after performing analytical continuation,

$$\Sigma_2(\vec{q},\omega)=\left(\frac{|E_b|^2\Phi t}{W\gamma}\right)\left(\frac{x_{\vec{q}}-2(t_{\vec{q}}-\mu)-\mu_B}{2x_{\vec{q}}}\right)\times\left(\frac{1}{\omega-1/2(x_{\vec{q}}-\mu_B)+i0^+}\right) + \frac{U^2\omega_c}{W}\left(\frac{x_{\vec{Q}-\vec{q}}-2(t_{\vec{Q}-\vec{q}}-\mu)-\mu_B}{2x_{\vec{Q}-\vec{q}}}\right)\times\left(\frac{1}{\omega+2\mu+|U|-1/2(x_{\vec{Q}-\vec{q}}+\mu_B)+i0^+}\right), \tag{40}$$

where ω_c is a frequency cutoff needed by the assumption that the η resonance is sharp for $(\vec{Q}-\vec{q})^2/4m^*\leq\omega_c\approx U^2/W$, with $m^*=m(|U|/t)$. This corresponds to $|\vec{Q}-\vec{q}|\lesssim U/W$, as it is borne out by numerical calculations of the

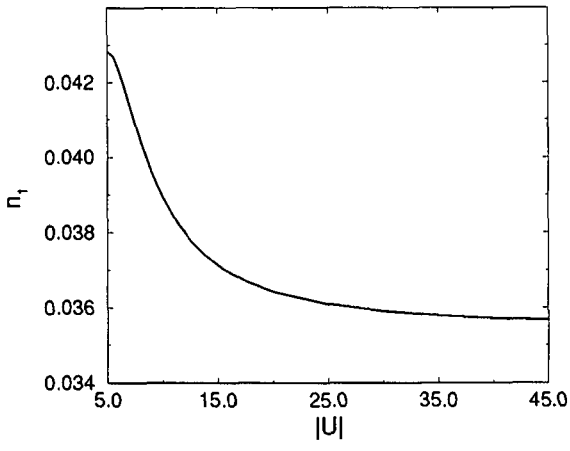

FIG. 3. Particle density n_1 which is obtained by using Eq. (25); the chemical potential is calculated numerically out of Eq. (32). The temperature is $T/t=0.5$.

two-particle Green's function $G^{(2)}$ covering the whole Brillouin zone.[12,18] The precise value of the cutoff has little influence in the following (numerical) results. We note that the first contribution in Eq. (40) is following from the long-wavelength behavior of the T matrix, while the second is due to the η resonance. Even though both Σ_1 and the first contribution to Σ_2 originate from the pole of $T_0(\vec{q},i\nu_n)$, given in Eq. (12), they are found to have opposite dispersions. The total self-energy results as

$$\Sigma(\vec{q},\omega)=\Sigma_1(\vec{q},\omega)+\Sigma_2(\vec{q},\omega). \tag{41}$$

At this point of the calculation, we can recalculate the particle density n_1 by evaluating explicitly Eq. (25), using the Green's function resulting from Eq. (41). Since there is no *a priori* reason that this would yield a result comparable to what is following from Eq. (32), this is a consistency check of the framework we are using. The result is displayed in Fig. 3. It is obvious that this is in very good agreement with the expected value $n=0.04$ for all values of U. This means that our calculation is consistent. It also implies that, on one hand, a small change in the chemical potential corresponds to a small change in the particle density, but on the other hand, it may induce a big change in the pair density.

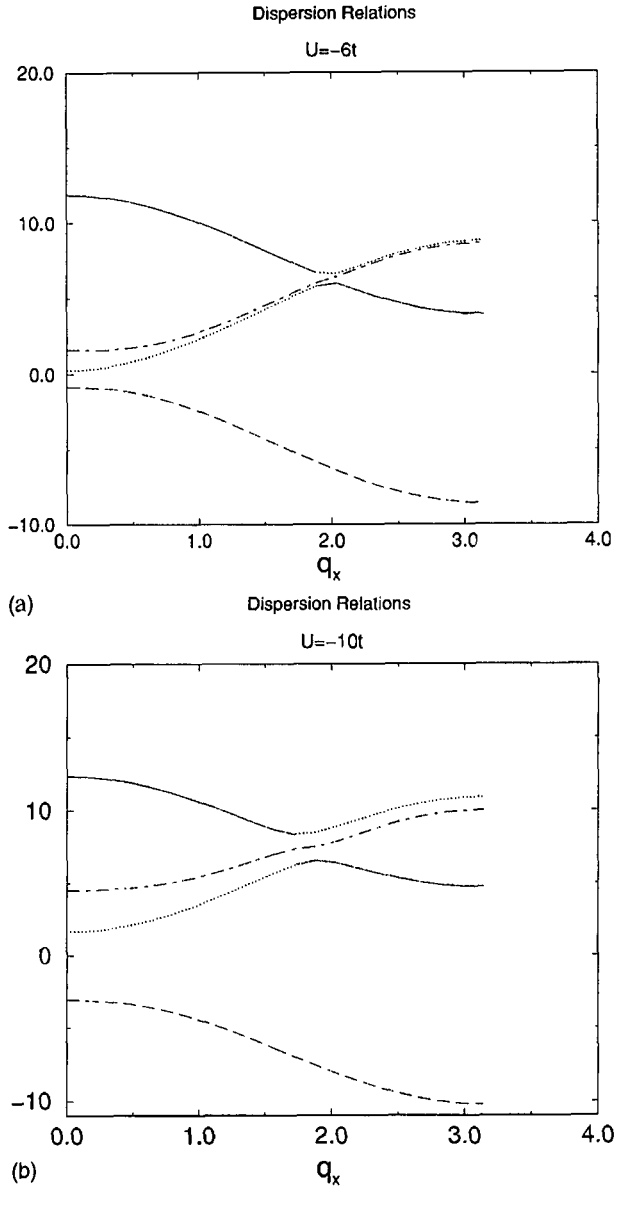

FIG. 4. (a) Spectrum of the Green's function at $n=0.04$, $T/t=0.1$, and $U=-6t$. It consists of the bosonic band (dashed line), the fermionic bands (dotted and dashed-dotted lines), and the η resonance band (full line). (b) The same as (a), for $U=-10t$ and $n=0.1$.

III. EXCITATION SPECTRUM

We can now summarize our findings by plotting the various pieces of the spectral function. This is done in Fig. 4(a), for $U=-6t$ ($E_b=-t$) and $n=0.04$, and in Fig. 4(b) for $U=-10t$ ($E_b=-4.2t$) and $n=0.1$, for momenta along the diagonal of the Brillouin zone. In both cases, the spectrum consists of four branches. The spectral weights of the various branches are displayed in Fig. 5(a) for $U=-6t$ and $n=0.04$ and Fig. 5(b) for $U=-10t$ and $n=0.1$.

These results can be commented as follows:

(i) There is a branch at negative energies following from the quasibound states. It is centered around $-W/2-(\Delta+|E_b|)/4$ with a width $W-(\Delta-|E_b|+2\mu_B)/2<W$. The dependence in U is weak, and the dispersions for $|U|=6t$ and $|U|=10t$ are essentially the same (at same densities), up to a small shift; moreover, we note that they are opposite to the free fermion dispersion. The weight decreases with increasing momentum and gets mostly negligible for $q_x\sim 2$. It decreases with increasing $|U|$, at small $\vec{q}$'s, but the total weight remains constant.

(ii) The fermionic band that was coming out of the first approximation [Eq. (18)] is now resulting as a superposition of two branches which would merge into a single one, were damping taken into account. This superposition is done out of the two branches which are most free-electron-like. This is somewhat arbitrary, especially in the domain where the hybridization with the other branch, which lies at positive energies too (see below), is strong. Consequently, we do not show the spectral weights in this range. The width of the

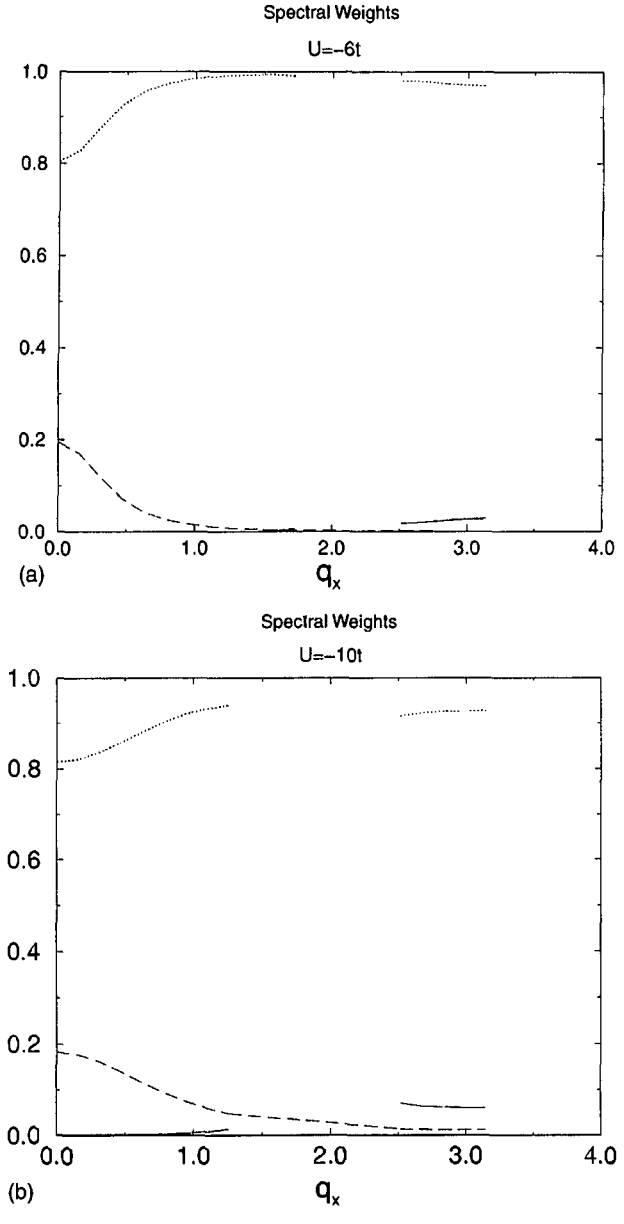

FIG. 5. (a) Spectral weight of the bosonic band (dashed line), the fermionic bands (dotted line) and the η resonance band (full line), for $n=0.04$, $T/t=0.1$, and $U=-6t$. (b) The same as (a) for $U=-10t$ and $n=0.1$.

fermionic band is slightly larger than the original bandwidth, and shows little dependence on U. Its dispersion is parallel to the free fermion one.

(iii) There is a third branch resulting from the η resonance; its dependence in U is weak and both curves (for $|U|=6t$ and $|U|=10t$) are parallel. It comes down in energy with increasing $|U|$. The contribution of the η resonance band is very small, barely accounting for 5–10% of the spectral weight at its maximum, which is located near $\vec{q}=\vec{Q}$.

It is interesting to compare our results with quantum Monte Carlo (QMC) simulations.[11,21] The calculations of Ref. 11 have been performed for $n=0.4$ and for $|U|=-4t,-8t,-12t$. This is likely to be outside the realm of densities for which the T-matrix approximation is really valid. Nevertheless, the following features coincide with our findings: there are two distinct excitation branches which get more and more clearly separated by a gap when $|U|$ increases. The width of the two bands is smaller than in our calculation, in particular the lower (bosonic) band has very little dispersion. However, the weights (the fermionic band has large weight for large wave vectors, whereas the weight of the negative energy bosonic band is concentrated near the zone center) is similar to our Figs. 4 and 5.

Reference 21 presents new results for the one-electron spectral function for $n=0.1$, one of the density values that we have used, and $|U|=8t$. Here again, there is a fermionic branch at positive energies E (positive with respect to the chemical potential), separated by a "pseudogap" from the excitations at $E<0$. Weight and width of the fermionic band is similar to our result. The excitations at $E<0$ have most weight near the zone center, as we find it. However, their structure seems to be more complex: with increasing wave number they split into two "subbranches." The lower part has downward dispersion and seems to correspond to our bosonic branch. The other subbranch produces weight near the chemical ($E\simeq 0$) potential for large wave numbers. This might correspond to our η resonance, provided that its energy near the zone corner, lying at a positive energy in our calculation, would in reality be lower. In this respect, the spectral functions for $n=0.4$ and $|U|=-6t$, also shown in Ref. 21, are particularly interesting: for $E>0$, besides the strong fermionic branch, there is a second branch of excitations the dispersions of which are very similar to the η peak in our Figs. 4 and 5.

Thus, the main features of our spectral functions seem to be present in the Monte Carlo results, although the latter show a more complex structure. A detailed and more quantitative comparison with QMC should also take into account the fact the "maximum entropy method" used there in order to extract spectral functions from data obtained as functions of the (imaginary) Matsubara frequencies does not easily allow for an unambiguous identification of excitations with small weight.

Finally, we note that we do not obtain any spectral weight at zero frequency, signaling the presence of a correlation induced gap. We also checked that including particle-hole excitations in the calculation does not affect this conclusion. The appearance of a true gap in our calculation is, at least partly, due to the fact that our spectral lines have no width (except that the "doubling" of the fermionic branch gives a hint to a broadening of the latter). Spectral functions with finite line width would be obtained either by doing the $\vec{q}$ sums in the expression (4) for the self-energy more precisely, and/or by evaluating G and Σ by solving Eqs. (2)–(5) self-consistently.

In summary, we have determined the excitation spectrum of the attractive Hubbard model at intermediate coupling out of a simple analytical calculation. We first pointed out an intrinsic problem of perturbation theory relative to the implementation of the Mermin-Wagner theorem. We made use of an alternative expression for the density to obtain a qualitatively correct theory which does not break down at low T in two dimensions, in contrast to previous self-consistent calculations. We obtain an analytical expression for the Green's function which reproduces the qualitative features of the QMC simulations in the low-density regime.

ACKNOWLEDGMENTS

We acknowledge valuable discussions with T. Schneider, J. M. Singer, M. H. Pedersen, and J. J. Rodríguez-Núñez. We thank J. M. Singer for providing us with his numerical data prior to publication. This work was financially supported by the Swiss National Science Foundation, under Grants No. 20-43111.95 and No. 20-47149.96. M.Yu.K. acknowledges the University of Neuchâtel, where part of this work has been performed, for hospitality and the Swiss National Science Foundation for partial funding.

[1] P. Nozières and S. Schmitt-Rink, J. Low Temp. Phys. **59**, 195 (1985).

[2] M. Drechsler and W. Zwerger, Ann. Phys. (Leipzig) **1**, 15 (1992).

[3] M. Randeria, N. Trivedi, A. Moreo, and R. T. Scalettar, Phys. Rev. Lett. **69**, 2001 (1992); N. Trivedi and M. Randeria, *ibid.* **75**, 312 (1995).

[4] Th. Meintrup, T. Schneider, and H. Beck, Europhys. Lett. **31**, 231 (1995).

[5] V. M. Galitskii, Sov. Phys. JETP **7**, 104 (1958); D. M. Eagles, Phys. Rev. **186**, 456 (1969); P. Bloom, Phys. Rev. B **12**, 125 (1975).

[6] J. R. Engelbrecht and M. Randeria, Phys. Rev. Lett. **65**, 1032 (1990); H. Fukuyama, Y. Hasegawa, and O. Narikiyo, J. Phys. Soc. Jpn. **60**, 2013 (1991).

[7] R. Frésard, B. Glaser, and P. Wölfle, J. Phys.: Condens. Matter **4**, 8565 (1992).

[8] R. Micnas, M. H. Pedersen, S. Schafroth, T. Schneider, J. J. Rodríguez-Núñez, and H. Beck, Phys. Rev. B **52**, 16 223 (1995).

[9] R. Haussmann, Z. Phys. B **91**, 291 (1993).

[10] P. J. H. Denteneer, G. An, and J. M. J. van Leeuwen, Phys. Rev. B **47**, 6256 (1993).

[11] J. M. Singer, M. H. Pedersen, T. Schneider, H. Beck, and H. G. Matuttis, Phys. Rev. B **54**, 1286 (1996); J. M. Singer, M. H. Pedersen, and T. Schneider (unpublished); J. M. Singer (private communication).

[12] M. H. Pedersen, Ph.D. thesis, University of Zurich, 1996; M. H. Pedersen, J. J. Rodríguez-Núñez, H. Beck, T. Schneider, and S. Schafroth, Z. Phys. B **103**, 21 (1997).

[13] B. R. Bulka and S. Robaszkiewicz, Phys. Rev. B **54**, 13 138 (1996); B. Bulka, *ibid.* (to be published).

[14] T. Schneider, M. H. Pedersen, and J. J. Rodríguez-Núñez, Z. Phys. B **100**, 263 (1996).

[15] See, for example, S. Schafroth, J. J. Rodríguez-Núñez, and H. Beck, J. Phys.: Condens. Matter **9**, L111 (1997); J. J. Rodríguez-Núñez (private communication).

[16] C. N. Yang, Phys. Rev. Lett. **63**, 2144 (1989).

[17] E. Nowak, Z. Phys. B **45**, 173 (1981).

[18] E. Demler, S. C. Zhang, N. Bulut, and D. J. Scalapino, Int. J. Mod. Phys. B **10**, 2137 (1996).

[19] Y. M. Vilk, L. Chen, and A.-M. S. Tremblay, Phys. Rev. B **49**, 13 267 (1994); Physica C **235-240**, 2235 (1994).

[20] Y. M. Vilk and A.-M. S. Tremblay, Europhys. Lett. **33**, 159 (1996); J. Phys. I **7**, 1309 (1997).

[21] J.M. Singer and T. Schneider (private communication).

Pseudogap in the one-electron spectral functions of the attractive Hubbard model

Massimiliano Capezzali and Hans Beck
Physics Institute
University of Neuchâtel
Rue A.L. Breguet 1
2000 Neuchâtel
Ch-Switzerland

We calculate the one-electron Green's function of the 2D attractive Hubbard model by coupling the electrons to pair fluctuations. The latter are approximated by homogeneous amplitude fluctuations and phase correlations corresponding to the XY-model. The electronic density of states shows a pseudogap at temperatures well above the transition temperature T_C. For a quasi-3D system, a superconducting gap emerges out of the pseudogap below T_C.

The 2D attractive Hubbard model is treated by a Stratonovich-Hubbard transformation (SHT), decoupling the interaction term by a complex pairing field Δ. The one-electron Green's function is then approximately given by [1]:

$$G\left(\vec{k},z_\nu\right)^{-1} = z_\nu - \epsilon_{\vec{k}} + \mu - \sigma\left(\vec{k},z_\nu\right) - \frac{\langle\Delta\rangle^2}{z_\nu + \epsilon_{\vec{k}} - \mu + \sigma\left(\vec{k},-z_\nu\right)}. \tag{1}$$

The expression for the self-energy

$$\sigma\left(\vec{k},z_\nu\right) = -\sum_{\vec{q}}\sum_{z_\alpha}\left\langle\left|\Delta\left(\vec{q},z_\alpha\right)\right|^2\right\rangle G\left(\vec{k}-\vec{q},z_\nu - z_\alpha\right), \tag{2}$$

involves the dynamic correlation function of the pairing field, which is related to the one-electron propagator through the SHT. However, rather than aiming at a self-consistent solution, we adopt a simple form for the pairing correlations and study their influence on the one-electron properties. Introducing amplitude and phase, $\Delta\left(\vec{r},t\right) = \left|\Delta\left(\vec{r},t\right)\right| e^{i\theta\left(\vec{r},t\right)}$, we make the following assumptions :

(i) Below the temperature T^*, the amplitude fluctuations (assumed to be space- and time-independent) are approximated by a BCS-form, $\left\langle|\Delta|^2\right\rangle = \Phi_0\left(1-\frac{T}{T^*}\right)$, with a prefactor Φ_0 that allows to vary their strength. The average $\langle\Delta\rangle$ is zero. The strong anisotropy of underdoped compounds shows that the coupling between the planes is weak. Thus, we model the phase fluctuations as in a 2D-XY system. Above the critical temperature T_C, we approximate it by a dispersionless relaxation [2,3] :

$$\left\langle e^{i\left(\theta\left(\vec{r},t\right)-\theta\left(\vec{0},t\right)\right)}\right\rangle = e^{-\gamma t}\left(\frac{r_0}{r_0+r}\right)^{\eta(T)} e^{-\frac{r}{\xi_+(T)}}, \tag{3}$$

with a Berezinskii-Kosterlitz-Thouless correlation length $\xi_+(T) = \xi_0 e^{\frac{b}{\sqrt{T-T_C}}}$ and a relaxation frequency γ.

(ii) Below the critical temperature T_C we keep, for simplicity, the same form (3) for the phase correlations, but with $\xi^{-1} = 0$, corresponding to an algebraic decay of correlations. Taking into account a non-zero coupling between the planes (in the third dimension), we introduce a non-zero value for the average of Δ, $\langle\Delta\rangle^2 = \lambda\left\langle|\Delta|^2\right\rangle$, with a variable parameter $\lambda \leq 1$.

We then evaluate $\sigma\left(\vec{k},z_\nu\right)$ to lowest order by using the non-interacting Green's function and the isotropic spectrum $\epsilon\left(\vec{k}\right) = \frac{k^2}{2m} - \mu$ in expression (2). The wave-number integration is limited to an effective spherical Brillouin zone. The various parameters are chosen to describe high-T_C materials in the strongly underdoped regime, where the pseudogap is most pronounced : the (fixed) chemical potential $\mu = \frac{k_F^2}{2m}$ is taken to correspond to about 0.1 charge

carrier per site and $k_B T^* = \mu$, $T_C = \frac{T^*}{6}$.
On the figures, we show the electronic density of states $N(E)$ and some spectral functions for $\Phi_0 = 0.76$ and $\gamma = 0.5\mu$. The following observations can be made :

(i) Above T_C, a pseudogap opens around μ. Its effective width is almost T-independent, in spite of the T-dependence of $\langle|\Delta|^2\rangle$ in the self-energy. Near T^*, it is roughly V-shaped. By approaching T_C, it becomes more U-shaped (for our model, pairing is s-like) and $N(\mu)$ becomes then practically zero; the pseudogap is delimited by two rather pronounced maxima, although $\langle\Delta\rangle$ is still zero.

(ii) Below T_C, the presence of $\langle\Delta\rangle \neq 0$ produces two new peaks: a true "superconducting gap" emerges out of the pseudogap. Its width is given by the geometrical superposition of average and fluctuating part of Δ. The fluctuations of the latter remain visible in the form of secondary shoulders inside the superconducting gap which approach each other about in the same proportion as the main peaks move away from each other.

(iii) Our value for γ is relatively large. For a smaller γ, and in particular in the case of critical slowing down of phase fluctuations ($\gamma\,(T_C^+) = 0$) [2] the two shoulders would become secondary peaks inside the superconducting gap.

(iv) Near T_C, the spectral functions are doubly peaked in some wave-vector domain around k_F and the width of the pseudogap is given by the separation between these two peaks, which is essentially determined by $\langle|\Delta|^2\rangle$. At higher temperatures, the spectral functions have only one peak, but their width is enhanced over essentially the same k-domain. Due to this fact, the pseudogap is filling up gradually, when T^* is approached (from below), without changing very much its width.

Summarizing, we have evaluated the electronic density of states of the attractive Hubbard model, taking into account the coupling of the charge carriers to the fluctuating pairing field. The appearance of a pseudogap with a T-independent width and the emergence of a superconducting gap below T_C is in agreement with experimental findings (see for example [4]). In a future publication, we shall present more detailed results and also compare the latter with the ones that have been recently proposed within similar approaches [5].

---

[1] M.H. Pedersen et al., Z. Phys. B **103** (1997), 21.
[2] D.L. Huber, Phys. Lett. A **68** (1978), 125.
[3] P.H.E. Tiesinga et al., Phys. Rev. Lett. **78** (1997), 519.
[4] Ch. Renner et al., Phys. Rev. Lett **80** (1998), 149.
[5] M. Franz and A.J. Millis, cond-mat/9805401; J. Maly et al., cond-mat/9805018; V.M. Loktev and S.G. Sharapov, Cond. Mat. Phys. (Lviv) **11** (1997), 131; M. Letz and R.J. Gooding, cond-mat/9802107; J.R. Engelbrecht and A. Nazarenko, cond-mat/9806223.

FIGURE CAPTIONS

Figure 1 : One-electron density of states $N(E)$ above T_C, for $T = 2T_C$ (dot-dashed line), $T = 1.5T_C$ (dotted line), $T = 1.2T_C$ (dashed line) and $T = 1.01T_C$ (full line).

Figure 2 : $N(E)$ below T_C for $\lambda = 0.7$ (full line) and - for comparison - above T_C ($T = 1.01T_C$, dashed line).

Figure 3 : One-electron spectral functions for $k = 0.5k_F$ (dashed line), $k = 0.7k_F$ (dotted line), $k = k_F$ (full line), $k = 1.2k_F$ (dash-dotted line), $k = 1.5k_F$ (heavy full line), for $T = 1.01T_C$ and (inset) $T = 1.5T_C$.

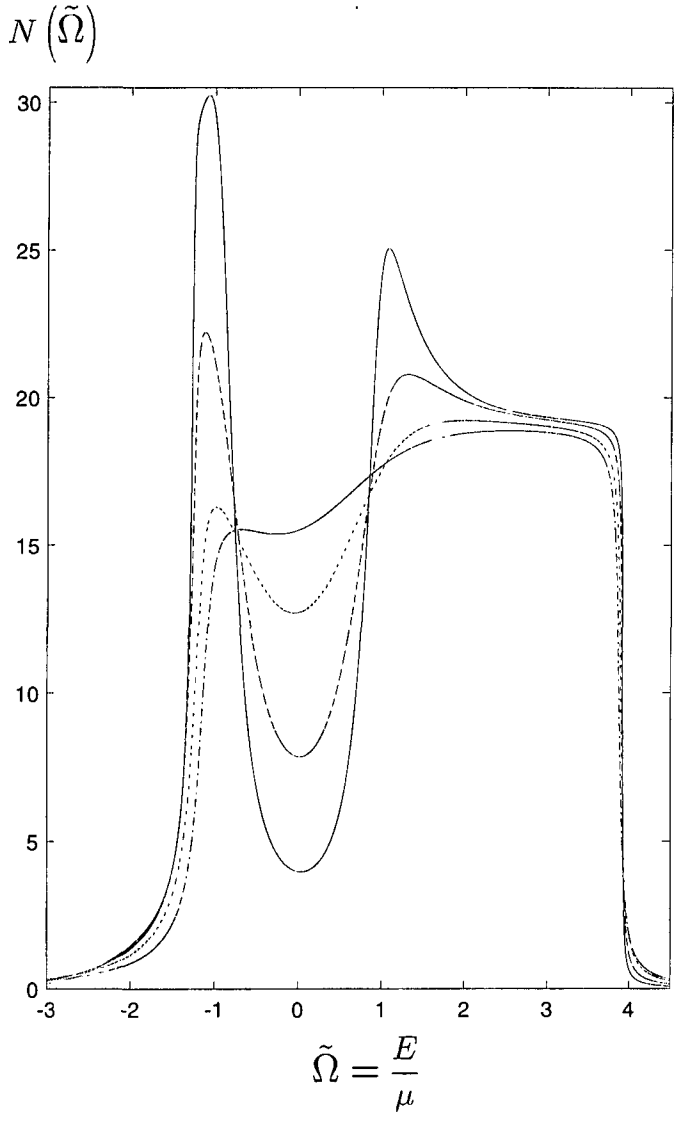

FIG. 1. One-electron density of states $N(E)$ above T_C, for $T = 2T_C$ (dot-dashed line), $T = 1.5T_C$ (dotted line), $T = 1.2T_C$ (dashed line) and $T = 1.01T_C$ (full line).

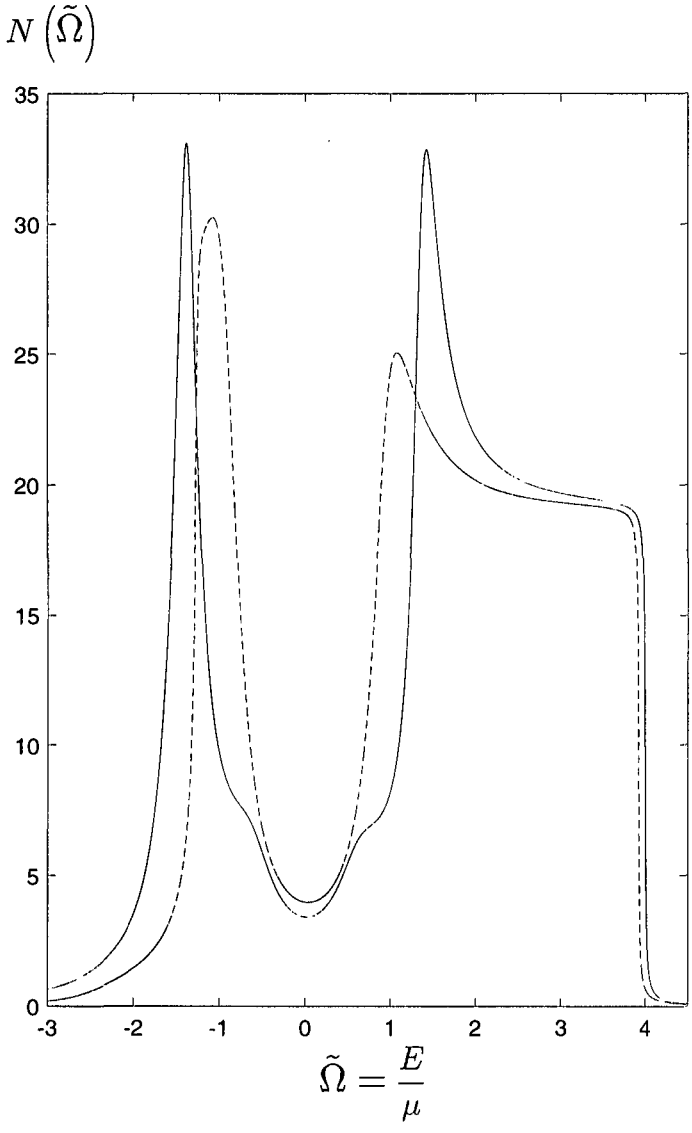

FIG. 2. $N(E)$ below T_C for $\lambda = 0.7$ (full line) and - for comparison - above T_C ($T = 1.01T_C$, dashed line).

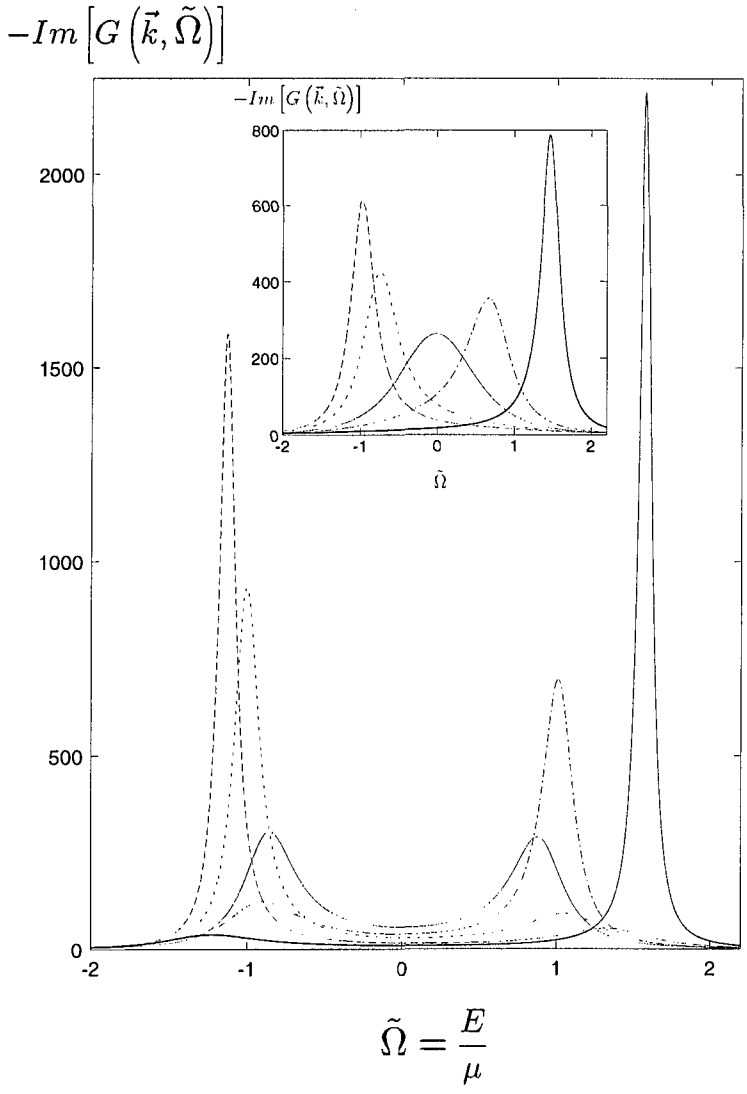

FIG. 3. One-electron spectral functions for $k = 0.5k_F$ (dashed line), $k = 0.7k_F$ (dotted line), $k = k_F$ (full line), $k = 1.2k_F$ (dash-dotted line), $k = 1.5k_F$ (hevay full line), for $T = 1.01T_C$ and (inset) $T = 1.5T_C$.

Excitation spectrum of the two-dimensional attractive Hubbard model

Massimiliano Capezzali and Hans Beck
Physics Department, University of Neuchâtel,
Rue A.L. Breguet 1, 2000 Neuchâtel, CH-Switzerland

We calculate the one-particle spectral functions above the superconducting transition temperature T_C, in the framework of a functional integral approach. The coupling of the electronic self-energy to pair fluctuations, which are treated by means of a time-dependent Ginzburg-Landau equation, yields a double-peak structure, around the Fermi wavenumber. The peak separation is essentially temperature-independent, but the structure sharpens when T_C is approached.

Although the two-dimensional attractive Hubbard model does not represent a suitable model to describe the complex physical behavior of the high-temperature superconducting compounds, it has recently attracted renewed interest [1–3], on one hand because of its simplicity and, on the other hand, because it incorporates two fundamental properties of the cuprate superconductors : working in two dimensions permits to take into account the strong anisotropy of the latter materials (at least in the underdoped regime), while the on-site attraction can account for the characteristic short in-plane coherence length, which has been experimentally determined.
In a previous paper [4], we calculated the one-electron Green's function of the two-dimensional attractive Hubbard model, by coupling the charge carriers to pair fluctuations, which were subsequently approximated by a homogeneous amplitude and by phase fluctuations, corresponding to the 2D-XY model; we found that the electronic density of states shows a pseudogap at temperatures well above the superconducting transition temperature T_C.
In the present communication, we shall treat pair fluctuations above T_C by means of a time-dependent Ginzburg-Landau equation. In order to derive the latter, the interaction term appearing in the Hamiltonian of the attractive Hubbard model is decoupled by a standard Stratonovich-Hubbard transformation, through which a complex, fluctuating pairing field Δ appears. The partition function is thereafter written as the functional integral, over the latter field, of an effective action which, upon exploiting the usual cumulant expansion for expectation values up to fourth order in Δ, becomes a dynamic Ginzburg-Landau-like functional, $S(\Delta)$. The expectation value of the squared modulus of the pairing field Δ has the form :

$$\Xi(\vec{q}, z_\alpha) \equiv \langle \mid \Delta(\vec{q}, z_\alpha) \mid^2 \rangle = \frac{1}{a + cq^2 + (d_1 + id_2) z_\alpha}, \quad (1)$$

where a, c, d_1 and d_2 are real coefficients that emerge from expanding the inverse of the two-particle propagator, for small wavenumbers $\vec{q}$ and (bosonic Matsubara) frequencies z_α. To lowest order, the self-energy is given by [4] :

$$\sigma(\vec{k}, z_\nu) = -\sum_{\vec{q}, z_\alpha} \langle \mid \Delta(\vec{q}, z_\nu) \mid^2 \rangle \, G_0(\vec{k} - \vec{q}, z_\nu - z_\alpha) =$$
$$\frac{1}{2\pi} \sum_{\vec{q}} \int_{-\infty}^{+\infty} Im\left[\Xi(\vec{q}, \zeta)\right] G_0(\vec{k} - \vec{q}, \zeta - z_\nu) n_B(\zeta) d\zeta -$$
$$\frac{1}{2\pi} \sum_{\vec{q}} \int_{-\infty}^{+\infty} \Xi(\vec{q}, z_\nu + \eta) Im\Big[G_0(\vec{k} - \vec{q}, \eta)\Big] n_F(\eta) d\eta, \quad (2)$$

where $n_B(\omega)$ and $n_F(\omega)$, respectively, are the usual Bose-Einstein and Fermi distribution functions.
Contrary to the self-consistent T-matrix approach [5], the self-energy given by Eqn. (2) involves the non-interacting one-particle Green's function $G_0(\vec{k}, z)$ [6] : on one hand, this choice provides us with analytically tractable expressions while, on the other hand, it should give physically reasonable results, because approximations which include self-consistency without the necessary vertex corrections are unable to reproduce the precursor effects [1], which we aim at putting in evidence. We use the isotropic spectrum $E(\vec{k}) = \frac{k^2}{2m} - \mu$. For the values of the Ginzburg-Landau parameters a and c, we use the strong-coupling limit [6,7], whereas we determine d_1 and d_2 from the best fit to the T-matrix resulting from Monte-Carlo calculations [6,5]. The imaginary part of the self-energy is shown on Fig. 1, for two temperatures above the transition temperature, which is defined by $a(T_C) = 0$. We have chosen $T_C = 0.1t$ (t is the hopping parameter of the original Hubbard Hamiltonian), in agreement with T-matrix calculations [5] and numerical simulations [3]. A transition at a non-zero temperature (which is also observed in Quantum Monte Carlo calculations, due to finite size effects [3]) would either have to be identified with a Berezinskii-Kosterlitz-Thouless transition or as being due to a small coupling in the third dimension. The most important features are the following : *(i)* the imaginary part of the self-energy shows a strong dependence upon wavenumber; upon increasing k, the rather pronounced peak moves down to the chemical potential, crosses it at $k = k_F$ and then continues down to lower energies; *(ii)* as the temperature increases, the imaginary part of the self-energy presents essentially the same structure, but the peaks get substantially broadened; *(iii)* for

large wavenumbers, $-Im\left[\sigma(\vec{k},\tilde{\Omega})\right]$ becomes almost featureless; this result probably arises from the fact that we have worked within the continuum limit while, on the lattice, the appearance of the so-called η-resonance would significantly modify the spectral properties at the edge of the Brillouin zone [8]; *(iv)* interestingly enough, we note that, except near the Fermi wavenumber, the imaginary part of the self-energy shows a minimum near the chemical potential, which, according to many authors [9], is a salient feature of a Landau Fermi liquid; however, for $k \sim k_F$, we note that a rather pronounced peak appears near the chemical potential.

The real part of the self-energy given by Eqn. (2) is computed by performing a Kramers-Kronig transformation; thereafter, the one-particle Green's function is obtained. In Fig. 2, we present the one-particle spectral functions for two different temperatures and for different wavenumbers. First of all, similarly to the case for the imaginary part of the self-energy, the spectral peaks broaden up, upon increasing the temperature above T_C; this is essentially the only effect and, in particular, we note that the position of the peaks does not change. Secondly, for the wavenumbers around k_F, the spectral function acquires a two-peak structure, which is symmetric with respect to the chemical potential for $k = k_F$. This feature persists to higher temperatures, though the thermal broadening tends to smear out the two-peaked structure.

On Fig. 3, we report the positions of the spectral peaks, which have a weight significantly different from zero. We note that, contrarily to the phase fluctuation approach that we presented in [4], the opening of a pseudogap, upon approaching T_C from above, is principally due to the double-peak structure around k_F.

Summarizing, we have computed the excitation spectrum emerging from the two-dimensional attractive Hubbard model, upon treating the pair fluctuations above T_C by means of a time-dependent Ginzburg-Landau equation. Around the Fermi wavenumber, the spectral functions exhibit a double-peak structure, the separation of which is essentially temperature-independent. Moreover, the spectral peaks sharpen when T_C is approached from above. The resulting one-particle density of states thus shows a pseudogap of almost constant width, above the superconducting transition temperature.

This work was supported by the Swiss National Science Foundation.

[1] Y.M. Vilk *et al.*, to be published in J. Phys. Chem. Sol., also cond-mat/9710013.
[2] M. Letz and R.J. Gooding, J. Phys. C **10** (1998), 6931.
[3] J.M. Singer *et al.*, submitted to Eur. Phys. J. B; R. Lacaze *et al.*, Eur. Phys. J. B **2** (1998), 509; J.R. Engelbrecht and A. Nazarenko, cond-mat/9806223; P.E. Kornilovitch and B. Kyung, cond-mat/9808107.
[4] M. Capezzali and H. Beck, cond-mat/9806211.
[5] R. Micnas *et al.*, Phys. Rev. B **52** (1995), 16223.
[6] The form of Eqn. (2) for the self-energy is obtained rigorously within the $O(n)$-model, for $N \to \infty$. See for example : M.H. Pedersen, Ph.D. Thesis, University of Zürich (Switzerland); M.H. Pedersen *et al.*, Acta Phys. Pol. **91** (1997), 419.
[7] M. Randeria, in *Bose Einstein Condensation*, A. Griffin *et al.* eds. (Cambridge University Press, Cambridge, 1994); M. Drechsler and W. Zwerger, Ann. Phys. **1** (1992), 15; S. Stintzing and W. Zwerger, Phys. Rev. B. **56** (1997), 9004.
[8] M. Yu. Kagan *et al.*, Phys. Rev. B **57** (1998), 5995.
[9] See for example : J. Maly *et al.*, cond-mat/9805018.

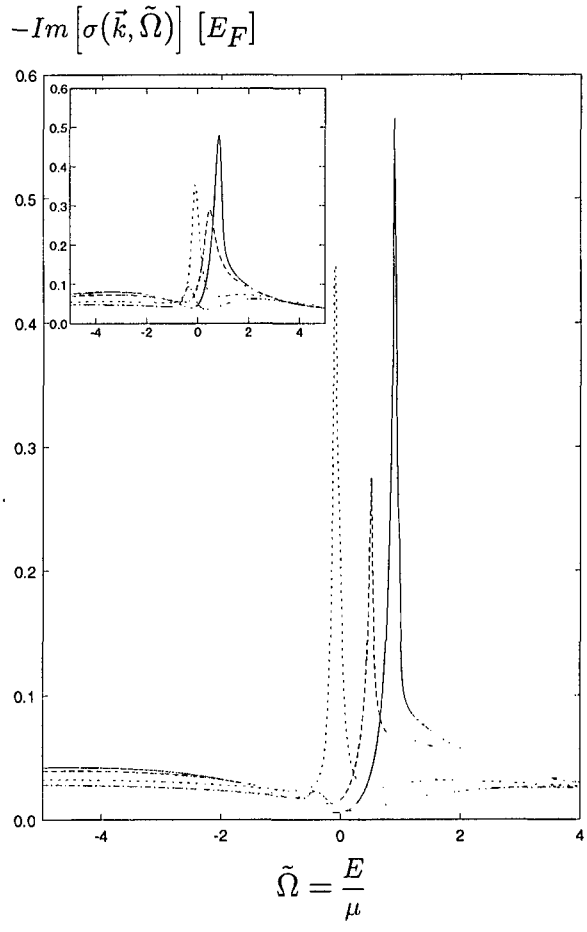

FIG. 1. Imaginary part of the self-energy, as calculated from Eqn. (2), in units of the Fermi energy E_F, for $k = 0.1k_F$ (full line), $k = 0.5k_F$ (dashed line), $k = 1.1k_F$ (dotted line), $k = 1.5k_F$ (dash-dotted line), for $T = 0.11t$ and, in the inset, for $T = 0.17t$. The chemical potential is the same for both temperatures and it is taken to correspond to about 0.1 charge carriers per site.

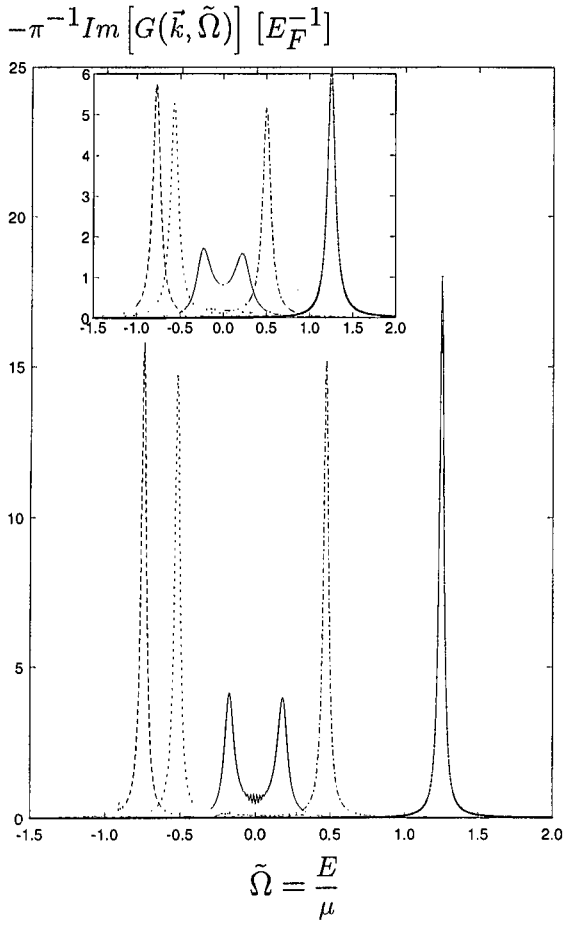

FIG. 2. One-particle spectral functions for $k = 0.5k_F$ (dashed line), $k = 0.7k_F$ (dotted line), $k = k_F$ (full line), $k = 1.2k_F$ (dash-dotted line), $k = 1.5k_F$ (heavy full line), for $T = 0.11t$ and (inset) $T = 0.17t$.

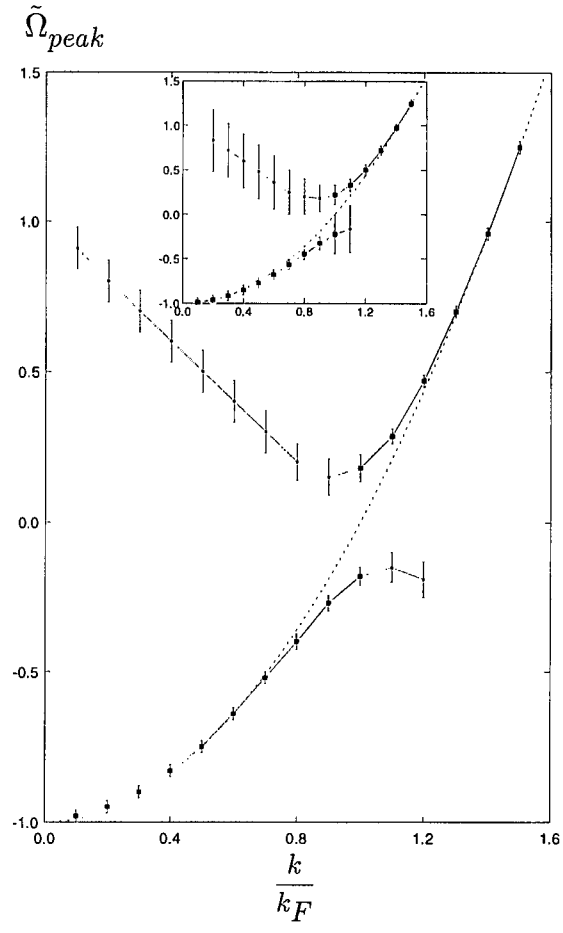

FIG. 3. Position of the spectral peaks for $T = 0.11t$ and, in the inset, for $T = 0.17t$. The big squares indicate the peaks that present a substantial spectral weight, while the small ones correspond to peaks with very small weight.

La version complète du manuscrit de la Thèse de doctorat a été déposée auprès de la Bibliothèque Centrale de l'Université de Neuchâtel et les publications ci-déposées en répresentent l'essentiel.

1) M. Capezzali, M. Mombelli, P. Béran et H. Beck, In *Macroscopic Quantum Phenomena and Coherence In Superconducting Networks*, C. Giovannella et M. Tinkham eds. (World Scientific, Singapore, 1995), pp. 270-277.
2) M. Capezzali, M. Mombelli et H. Beck, Physica B**222** (1996), pp. 304-308.
3) M. Capezzali, D. Ariosa et H. Beck, Physica B**230-232** (1997) pp. 962-965.
4) M. Capezzali, S.R. Shenoy et H. Beck, Phys. Rev. Lett. **78** (1997), pp. 523-526.
5) M. Yu. Kagan, R. Frésard, M. Capezzali et H. Beck, Phys. Rev. B **57** (1998), pp. -.
6) M. Capezzali et H. Beck, cond-mat/9806211, accepté pour publication dans Physica B.
7) M. Capezzali et H. Beck, cond-mat/9809349, accepté pour publication dans Physica C.